Geology of the Common Mouth of the Ares and Tiu Valles, Mars

A. G. Marchenko*, A. T. Basilevsky*, H. Hoffmann**,
E. Hauber**, A. C. Cook***, and G. Neukum**

* Vernadsky Institute of Geochemistry and Analytical Chemistry, Russian Academy of Sciences,
ul. Kosygina 19, Moscow, 117975 Russia
** DLR Institute of Planetary Exploration, 12489 Berlin, Germany
*** Center of Earth and Planetary Studies, National Air and Space Museum, Washington, DC, USA
Received June 23, 1998

Abstract—Since the *Mars Pathfinder* landing site is located at the mouth of the Ares and Tiu valles, this region attracts keen scientific interest. In order to better understand experimental data from this small area of the surface of Mars, which has been investigated by the rover, and the properties of the materials occurring here, it is necessary to answer how, from where, and when this material was transported. To answer these questions, we performed photogeological mapping and counted impact crater in the region. A photogeological analysis of 320 TV images of the studied area, thermal-inertia maps, and digital elevation models were used in mapping. Our results, and those published by other scientists, allow us to distinguish several principal stages in the geological history of the mouth of the Ares and Tiu valles: the destruction stage of an ancient plateau and three stages of fluvial activity. Deposits transported by water flows to the *Mars Pathfinder* landing site presumably consist of fragments of the material of ancient Martian highlands (impact breccias and lavas), of younger sedimentary or volcano–sedimentary material of ridged plains, of impact-crater materials, and of eolian products. The main constituents should be as old as approximately 4 Gyr (highland materials) and 3.5 Gyr (ridged-plain materials). It is very likely that the fluvial reworking of this ancient material took place between 3.6 and 2.6 Gyr ago and, possibly, even later, between 2.3 and 1.4 Gyr ago.

1. INTRODUCTION

1.1. Martian Outflow Valleys

In 1970, images obtained by *Mariner 9* revealed valleys on the Martian surface, which are similar in morphology to valleys and dry river channels on the Earth (McCauley *et al.*, 1972). The similarity is, however, incomplete; for example, many Martian valleys, in contrast to their terrestrial counterparts, lack drainage basins. Several morphological varieties of Martian valleys, such as valley networks, outflow valleys, runoff valleys, and fretted valleys, are distinguished (Sharp and Malin, 1975; Carr, 1996). The Ares and Tiu valles studied in this work are of the outflow-valley class. About 15 Martian valleys of this class are known at present (Baker, 1982); they all are large (up to several thousand kilometers long) and almost completely lacking in tributaries. In the recent geological epoch, water on Mars' surface could exist only in the form of ice and vapor, because the atmospheric pressure at the planet surface is only 5–10 mb. The outflow valleys were formed 3.6–0.5 Gyr ago after a period of heavy meteoritic bombardment, when atmospheric conditions were most likely similar to the current state (Masursky *et al.*, 1977; Scott *et al.*, 1979; Wise *et al.*, 1979; Baker and Kochel, 1979).

Large river valleys on the Earth evolve over millions of years, mainly under the control of atmospheric precipitation. Environments at the surface of Mars and the lack of drainage basins related to outflow valleys exclude this mechanism for their formation. Glacier movements represent another process forming valley-shaped landforms on the Earth. Some researchers (Lucchitta *et al.*, 1981; Lucchitta, 1982; Kargel *et al.*, 1995) believe this process was similarly responsible for the origin of the Martian outflow valleys. However, glaciers of the Earth usually move along the fluvial (water-formed) valleys, transforming them into glacial troughs (Hamblin, 1975). In addition, the growth, movement, and thawing (but not evaporation) of glaciers can proceed under terrestrial, but not under Martian atmospheric conditions.

According to some scientific ideas, a possible alternative is the catastrophic (geologically instantaneous) origin of outflow valleys, which was so quick that there was no time for water evaporation. In this case, we should assume an instantaneous release of a huge volume of water.

The outflow valleys could have been formed as a consequence of catastrophic outflows of ground water to the surface (Baker and Milton, 1974; Baker and Kochel, 1978; Carr, 1979). There is evidence for the idea that the Martian lithosphere may include horizons saturated with ice or water (see, for instance, Kuz'min, 1980). The morphology of head areas of outflow valleys is indicative of plentiful sinkholes. Several processes could provoke water outflows on the surface. According to a hypothesis by Carr (1979), this was a

pressure increase in water-bearing horizons due to freezing. Some scientists (McCauley *et al.*, 1972; Masursky *et al.*, 1977) assume water discharge to be a result of the thawing of permafrost under the influence of geothermal heating. Others believe that outflow valleys and their deposits were formed by the movement of a substance rich in solid material, resembling mud flows or lahars (Nummedal and Prior, 1981; Tanaka, 1988, 1997).

Features similar to the Martian outflow valleys are well known on the Earth (Milton, 1973; McCauley *et al.*, 1972). They are related in origin to catastrophic water release from glacier-dammed lakes (Bretz *et al.*, 1956; Bretz, 1969; Butvilovskii, 1993; Rudoi, 1995) and to ice thawing in response to volcanic eruptions under glaciers (e.g., Thörarinsson, 1957). These geomorphological features are rare terrestrial counterparts of the Martian outflow valleys, although the water-discharge values in the last case should be 10–100 times greater (Baker and Milton, 1974; Baker, 1982).

1.2. What is Stimulating Interest in the Mouth of the Ares and Tiu Valles?

Whatever the formation mechanism of outflow valleys—in particular, the Ares and Tiu—was (catastrophic fluvial, related to mudflows, or glacial), it obviously might involve the transport of the materials derived from geologically different regions of Mars cut by these valleys to the mouth of the flows. The Ares and Tiu valles begin in regions with a chaotic morphology of the ground-collapse type, then they run across an ancient, heavily cratered highland region, and finally open to the lower-laying Chryse Planitia, where they merge (Fig. 1a). Each of these valleys is about 1500 km long and 25–100 km wide. Thus, they are as long as the largest rivers of the Earth, e.g., the Amazon River, but are notably wider. Moreover, processes unrelated to the valley origin proper could also operate in their common mouth, being responsible for the influx of various materials, e.g., for sedimentation in temporary lakes and sea basins (Parker *et al.*, 1989, 1993; Baker *et al.*, 1991; Scott *et al.*, 1991; Craddock *et al.*, 1997), eolian accumulation (Kuzmin and Greeley, 1995a, 1995b), subsequent lava eruptions (Robinson *et al.*, 1996), and later mudflows (Jöns, 1984).

The high probability of detecting diverse geological materials in the Ares/Tiu mouth was the main reason for choosing this area for a detailed study with a moderate-sized rover brought by *Mars Pathfinder* (Golombek *et al.*, 1995, 1997b). In order to interpret the geological and geochemical characteristics of this area, we need to know how, from where, and when these materials were transported to the area in question.

To find answers to these questions we performed a geological mapping of the Ares/Tiu mouth, located from 15° to 30° N and 26° to 36° W (Fig. 1a) and suggested a scenario of its geological evolution.

1.3. Data Used and Investigation Methods

Geological mapping was performed using the photogeological analysis of TV images and some other data (Marchenko, 1996; Marchenko *et al.*, 1996, 1997, 1998). We used 320 images in the visible spectrum range obtained by the *Viking Orbiter*, thermal-inertia and rock-abundance maps compiled on the basis of the thermal-mapping data obtained by this spacecraft (Christensen, 1986; Christensen and Kieffer, 1989; Edgett and Christensen, 1997), along with a color mosaic of the images shot by this spacecraft through various photo-filters. The resolution of the *Viking* images is 36–821 m per pixel. The resolution of the thermal-mapping data used in this study is 30 km. In addition, a semiautomatic analysis of stereoscopic images (Thornhill *et al.*, 1993) was used to construct topographic maps of several areas and to evaluate the altitudes of some relief features. When the distinguished age (stratigraphic) units of the surface were marked by a statistically significant number of impact craters, their calculated density was used to check the age interpretation. The impact-crater count was performed on the basis of 55 images.

In our studies, we refer to the global and regional stratigraphy of Mars elaborated recently by other researchers. Scott and Carr (1978) were first to recognize three major stratigraphic-age units of this planet: Noachian (ancient), Hesperian (middle), and Amazonian (young). They also evaluated the crater densities characteristic of these units. The absolute age of the units is a point of controversy. Neukum and Wise (1976) defined the ages of the Noachian–Hesperian and the Hesperian–Amazonian boundaries as 3.8 and 3.6 Gyr, whereas Hartmann *et al.*, (1981) suggest that they are 3.5 and 1.8 Gyr old, respectively.

A map by Scott and Tanaka (1986), comprising the region under discussion, was used as a basis for our more detailed mapping. This map depicts more detailed stratigraphic subdivisions than that of Scott and Carr (1978), and each of the units is characterized by its impact-crater density. In our study, we distinguished several new stratigraphic units missing in the map by Scott and Tanaka (1986) and suggested a new interpretation to some others recognized before. Most detailed among the geological–geomorphologic maps comprising the studied region is that of Rotto and Tanaka (1995), although the stratigraphic and morphologic units of valley floors and eolian deposits, especially interesting for us, are missing there.

1.4. The Layout of the Paper

In section 2, we describe the distinguished geological (stratigraphic) units shown in our map. Some physical parameters of their surface are presented in section 3, and
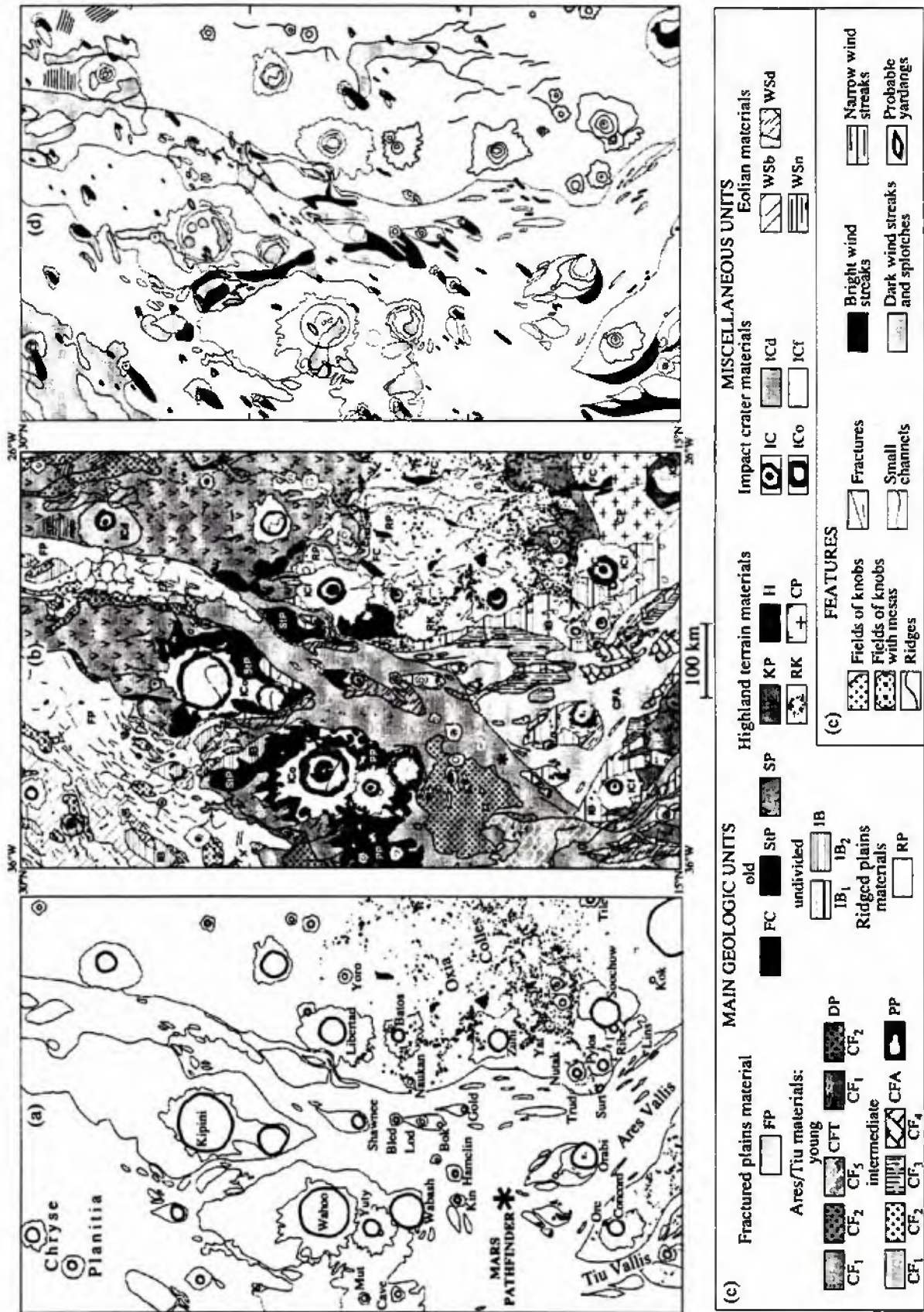
Fig. 1. Maps of the studied region and legends: (a) nomenclature of the principal landforms; (b) geological map; (c) legend for the geological map; (d) map of eolian deposits and forms; (e) legend for the map of eolian deposits and forms.
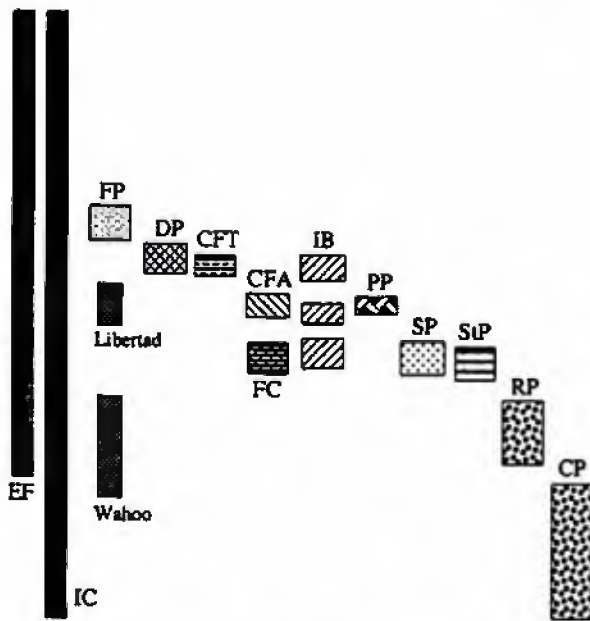
Fig. 2. Stratigraphic scheme proposed for the studied region. Right: subdivisions predating valley formation (CP, RP); center: units of the Ares and Tiu Valles floor (StP, SP, FC, IB, PP, CFA, CFT, DP) and fractured plains (FP); left: impact craters (IC) and eolian materials (EF); the (vertical) time scale is arbitrary. For symbol explanation see Fig. 1c and text.

our results of the impact-crater count are included in section 4. Correlation between these results and the data of photogeological analysis is discussed in section 5. The model ages for the distinguished stratigraphic units and events of their subsequent reworking are the main topics of section 6. In section 7, on the basis of our investigation, we present a scenario of the geological history of the area studied. Finally, section 8 is devoted to a general discussion of the materials from the *Mars Pathfinder* landing site in the context of this study.

2. DISTINGUISHED MATERIAL UNITS

2.1. Structure of This Section

On the basis of the photogeological analysis of images, crater counting, and previous publications, we distinguished 14 major geological subdivisions (stratigraphic units) in the region studied (Figs. 1b, 1c, 1d) and suggested their formation history (for the resulting stratigraphic scheme, see Fig. 2). The distribution of the images obtained by the *Viking Orbiter* (Figs. 4–15), which illustrate the morphology of these units in the region at hand, is shown in Fig. 16. Sometimes we refer to images that are missing from the set presented here. In this case, we indicate the image number according to the system of the *Viking Orbiter* catalog, e.g., 864A07. The impact-crater densities calculated for the identified stratigraphic units are listed in the table and are shown in Fig. 3. The standard crater-density values character-

istic of three major subdivisions of Martian stratigraphy are quoted after Scott and Tanaka (1986). The stratigraphic units are described, beginning with their oldest ones. We distinguish three major groups of units: (1) a group predating the formation of the Ares and Tiu valles; (2) the unit group of these valleys; and (3) the youngest group consisting of only the unit of fractured plains. The materials of impact craters and eolian deposits are considered to be formed over a time period longer than any of the mentioned age groups. The first and the second group are divided into subgroups, but within the latter, it is difficult to determine age relations between the units: they are different in morphology; however, it is not clear whether this is a result of differences in particular formation processes or of subsequent resurfacing. Within some units (valley floors, islands, and benches—see below) we also distinguish morphological types of the surface.

2.2. Ancient (Valley-Predating) Materials

The valley-predating geological subdivisions represent four groups of the highland-terrain materials and the younger material of ridged plains.

Highland stratigraphic units. *Cratered plateau* (CP, image 864A07) is a characteristic feature of the southeastern part of the region under study. It occupies an area with large, ancient, heavily destroyed impact craters. The plateau surface also exhibits random wrinkle ridges. The surface between the craters is spotted. Splotches are dark and rounded, up to 5–10 km in diameter. It is likely that the material in the splotches represents dark eolian deposits in the heavily destroyed craters. Several faint valleys in the plateau are 2–6 km wide and seemingly fluvial in origin. The CP material presumably includes the Middle Noachian impact breccias and the Hesperian–Noachian lavas (Rotto and Tanaka, 1995). During the Late Noachian time, before the origin of the Ares and Tiu valles, the plateau was destroyed in the north by slope-collapse events and under the influence of water-saturated mudflows (Squyres and Kasting, 1994; Tanaka, 1995). This stage of erosion appears to be related to the origin of the Great Northern Plain (McGill and Dimitriou, 1990). Later flows eroded the cratered plateau (CP) in the west to form the Ares Vallis. This plateau is likely the oldest in the region, because there are no data suggesting that its material overlies any other rocks. Our crater-counting results indicate a Noachian age for the plateau (Fig. 3).

Knobby plateaux (KP, Fig. 4) are typical of the south and southeast. They are quite similar to the cratered plateau (CP), but differ from the latter by the presence of numerous small knobs. Knobs are up to hundreds of meters across; they are larger in the north than in the south, and isometric in shape. Usually, these features show chaotic distribution patterns, but are locally arranged into chains and rings. It was suggested that knobs were created during the intense destruction of the northern highland margin at the end of the Noa-

Table. Areas of impact-crater counting

Site	*Viking Orbiter* images	Total area, km²	Map symbol	Coordinates of the complex-area center	Complex area, km²	Total number of craters[a]	Number of craters (of diameter >1 km) per 10⁶ km² ± 1 standard deviation	Model absolute age, Gyr
1	669A87-90	5742.35	IC Kipini	26.4N, 30.8W	279.27	13	8490 ± 5500	0.7 3.97
			SP	26.7N, 30.5W	3802.68	151	1540 ± 630	1.56 3.56
			IB₂	26.2N, 30.1W	292.55	13	–	0.87
			CFT (see 1 + 2)	26.2N, 30.4W	758.76	36	2380 ± 1757	1.06 2.89
			SC[b]	–	609.09	–	–	–
2	669A91-94	4532.15	StP	25.9N, 28.9W	106.50	6	–	–
			SP	26.9N, 30.8W	92.95	7	23920 ± 15985	3.55 4.06
			SP (see 2 + 3)	26.3N, 28.6W	196.46	9	–	–
			IB₂	26.8N, 29.2W	332.15	16	–	1.47
			CFT (see 1 + 2)	26.4N, 29.6W	913.22	57	3620 ± 1968	1.51 3.61
			FP	26.5N, 29.0W	1939.58	115	1031 ± 729	1.36
			FP	26.1N, 29.0W	654.83	63	4490 ± 2611	3.56
			SC	–	296.46	–	–	–
1 + 2			CFT			93		1.30 3.24
3	669A95-96	2123.79	StP	25.8N, 28.9W	35.32	3	–	–
			SP (see 2 + 3)	26.6N, 28.0W	1914.91	92	2780 ± 1205	0.94 1.52 3.95
			FP	26.7N, 28.7W	141.72	13	13650 ± 9790	–
			SC	–	31.84	–	–	–
2 + 3			SP			101		0.94 1.52 3.93
4	669A67-70	6802.31	IC	28.8N, 34.9W	736.73	26	–	1.50
			FP	28.7N, 35.3W	5557.69	246	2498 ± 668	2.01 3.61
			FP	28.5N, 35.1W	311.47	12	–	0.71
			SC	–	196.42	–	–	–
5	034A89-92	6095.43	IC[c]	24.4N, 32.1W	183.97	4	–	0.38
			IC Wahoo[d]	23.6N, 33.3W	361.56	18	5010 ± 3695	0.96 3.10
			IC Wahoo[e]	23.7N, 33.0W	1586.92	22	1060 ± 815	0.51
			StP	24.0N, 33.0W	1055.61	35	3425 ± 1800	1.21 3.98
			PP (see 5 + 6)	24.4N, 32.9W	992.45	26	–	0.68
			IB₂	24.6N, 32.2W	535.92	11	3710 ± 2630	0.34
			CFT	24.5N, 32.5W	1112.15	31	2961 ± 1628	0.86 3.63
			SC	–	266.85	–	–	–
6	034A83-84	3341.94	IC Mut and Cave	–	203.59	2	–	–
			PP (see 5 + 6)	22.5N, 35.1W	2861.16	74	1770 ± 780	0.95 2.22 2.97 3.74
			CFT	21.8N, 35.2W	151.50	6	1.40 E-3	2.83
			DP	23.0N, 35.5W	125.69	4	–	–
5 + 6			PP			100		0.87 2.22 3.67

Table. (Contd.)

Site	*Viking Orbiter* images	Total area, km²	Map symbol	Coordinates of the complex-area center	Complex area, km²	Total number of craters[a]	Number of craters (of diameter >1 km) per 10⁶ km² ± 1 standard deviation	Model absolute age, Gyr
7	633A41-44	11483.61	IC	24.4N, 27.6W	285.18	5	13420 ± 6850	4.17
			KP	22.5N, 27.0W	55.82	3	–	–
			SP	24.2N, 27.2W	1492.97	19	5580 ± 1932	3.88
			SP (see 7 + 9)	23.2N, 26.8W	9617.59	151	2640 ± 523	1.76 3.56 3.75
			SC	–	32.05	–	–	–
8	008A30-31	4252.72	IC Wahoo, ejecta	23.8N, 34.8W	35.90	3	27855 ± 27855	1.93
			StP and SP	24.0N, 34.8W	560.90	31	1783 ± 1783	1.05 2.69
			IB₂	24.0N, 35.1W	93.78	5	–	3.19
			DP (see 6 + 8)	23.7N, 35.5W	2655.40	119	1030 ± 616	1.51
			FP	24.2N, 35.4W	817.40	45	3030 ± 1910	2.20
			SC	–	89.34	–	–	–
6 + 8			DP			123		1.58
9	864A06-12	162170.5	NPL₁	18.0N, 24.0W	12767.21	79	6082 ± 690	3.87 4.05 4.17
			NPL₂	14.0N, 26.0W	16633.05	66	3915 ± 486	3.80 3.99 4.08
			CP	16.4N, 27.0W	28273.56	142	4940 ± 418	3.82 3.95
			KP	17.5N, 27.7W	16627.46	76	4480 ± 517	3.80 3.94
			IC Soochow	16.8N, 28.9W	4989.83	13	2577 ± 719	3.74 3.89
			IC Ribe	16.6N, 29.2W	426.22	2	–	3.94
			Soochow and Ribe			15		3.77 3.87
			IC Zuni	19.3N, 29.3W	2359.59	5	2099 ± 944	3.48
			IC Batos	21.7N, 29.5W	1413.03	5	3505 ± 1574	3.82
			IC Libertad	23.3N, 29.4W	2845.54	7	2393 ± 914	3.43
			RP	20.5N, 27.7W	44051.29	145	3230 ± 271	3.69 3.79
			IB₁	15.0N, 28.0W	9907.57	47	4676 ± 687	3.76 3.89
			CFA₄	13.0N, 28.0W	14433.95	19	1640 ± 378	3.52 3.75
			CFA₃	15.0N, 29.9W	1891.70	4	2080 ± 1046	3.09
			CFA₄ + CFA₃			23		3.48 3.71
			SP (see 7 + 9)	22.9N, 26.3W	7999.38	27	3270 ± 636	3.70 3.88
			SC	–	551.10	–	–	–
7 + 9			SP			178		3.57 3.79
10	004A49-54 and 003A43	8912.14	RP	20.8N, 30.4W	523.83	25	7330 ± 3740	2.69 3.79
			IB₁	20.9N, 31.5W	1373.63	65	5096 ± 1926	2.97 3.75
			CFA (see 10 + 11)	20.5N, 31.5W	6622.52	201	2869 ± 658	1.69 3.69 3.74
			SC	–	392.16	473	–	–

Table. (Contd.)

Site	Viking Orbiter images	Total area, km²	Map symbol	Coordinates of the complex-area center	Complex area, km²	Total number of craters[a]	Number of craters (of diameter >1 km) per 10⁶ km² ± 1 standard deviation	Model absolute age, Gyr
11	004A41-48	9872.70	IC	–	475.11	4	–	–
			IB$_1$	18.7N, 33.2W	21.22	4	–	3.62
			CFA + CFT (see 10 + 11)	19.5N, 32.8W	8695.65	296	2166 ± 498	1.57 3.46 3.74
			SC	–	680.72	–	–	–
10 + 11			CFA + CFT			497		1.62 3.59 3.74
12	004A19-23, 004A36, 004A40	8860.92	IB$_1$	18.2N, 33.6W	625.18	33	4799 ± 2770	3.23 4.00
			CFT	18.6N, 34.3W	7936.51	340	1323 ± 407	2.25
			SC	–	299.23	486	–	–

[a] Diameter greater than six pixels.
[b] Clusters of secondary craters.
[c] Crater rim.
[d] Crater floor.
[e] Ejecta, central rise, and rim.

chian time (Tanaka, 1995). That is probably why they are larger in size northward, where the erosion level was deeper. Rings of knobs apparently represent the destroyed rims of impact craters (RK, see below), whereas their chains are remnants of partially wrecked wrinkle ridges. The boundary between the units knobby (KP) and cratered (CP) plateaux is indistinct. We interpret the KP material as products of the terminal Noachian erosion of the cratered plateau (CP). Later flows that created the Ares and Tiu valles eroded the KP material.

Hills and mesas (H, Fig. 4) inside ridged and smooth plains (RP and SP, respectively—see below) represent frequent and specific features of the surface. Hills resemble the similar landforms of knobby plateaux, but are larger (1–2 km across on average). Flat-topped mesas up to 10 km in diameter have steep slopes and presumably are remnants of an ancient dismembered surface. The hills of unit H are more remote from one another than their analogues in the knobby plateaux.

A zone of hills and mesas, known as Oxia Colles, is about 160 km wide and extends from the southwest to the northeast in and outside the studied area. Mesas and hills of unit H seem to be remnants of an ancient cratered plateau (Rotto and Tanaka, 1995; Tanaka, 1995). Boundaries between them and other materials are concealed under slope deposits, and the age relationships of these materials remain obscure. It is only established in a few localities that foothill areas are overlain by flow-shaped deposits of very young fractured plains (FP, see below and in Fig. 5).

Rings of knobs (RK, Fig. 6) are seen in the images as rings or semicircles. These landforms are mostly concentrated inside the knobby plateaux and ridged plains, and only one ring is located much further to the north, in smooth plains (see below). It is evident that rings of knobs are remnants of the rims of large, ancient impact craters of the Noachian plateau (Rotto and Tanaka, 1995; Tanaka, 1995), and the material is thus the same in units RK, CP, and KP. The northernmost ring is located at a latitude of 30° N. According to Crumpler (1995), this position means that the material of the ancient plateaux is also present under the younger, smooth plains; in this case, the distribution area of the former extends northward up to 30° N.

Ridged plains (RP, Fig. 4) are located in the east of the studied region, north of the KP area. The boundary between units KP and RP is seen in the images as an escarpment or steep slope facing the RP area. Wrinkled ridges of submeridional orientation are characteristic features of these relatively bright plains. As already mentioned, within the ridged plains, there are relic hills (H) of a more ancient material. In addition, within these plains, several indistinct, valley-like landforms and elongated hills were detected, which are of submeridional orientation and are presumably composed of younger material of faint channels and islands (FC, see below). Because the ridged plains (RP) display wrinkle ridges at their surface, as is typical of many volcanic plains of Mars, the Moon, and Venus, some researchers believed that the ridged-plain material originated from lava eruptions (Scott and Tanaka, 1986; Rotto and Tanaka, 1995). However, neither boundaries nor vents of lava flows have been detected in the region. Watters (1988), as well as Rice and De Hon (1996) suggested that the wrinkle ridges could also be formed over a sedimentary substratum. We also share the opinion of
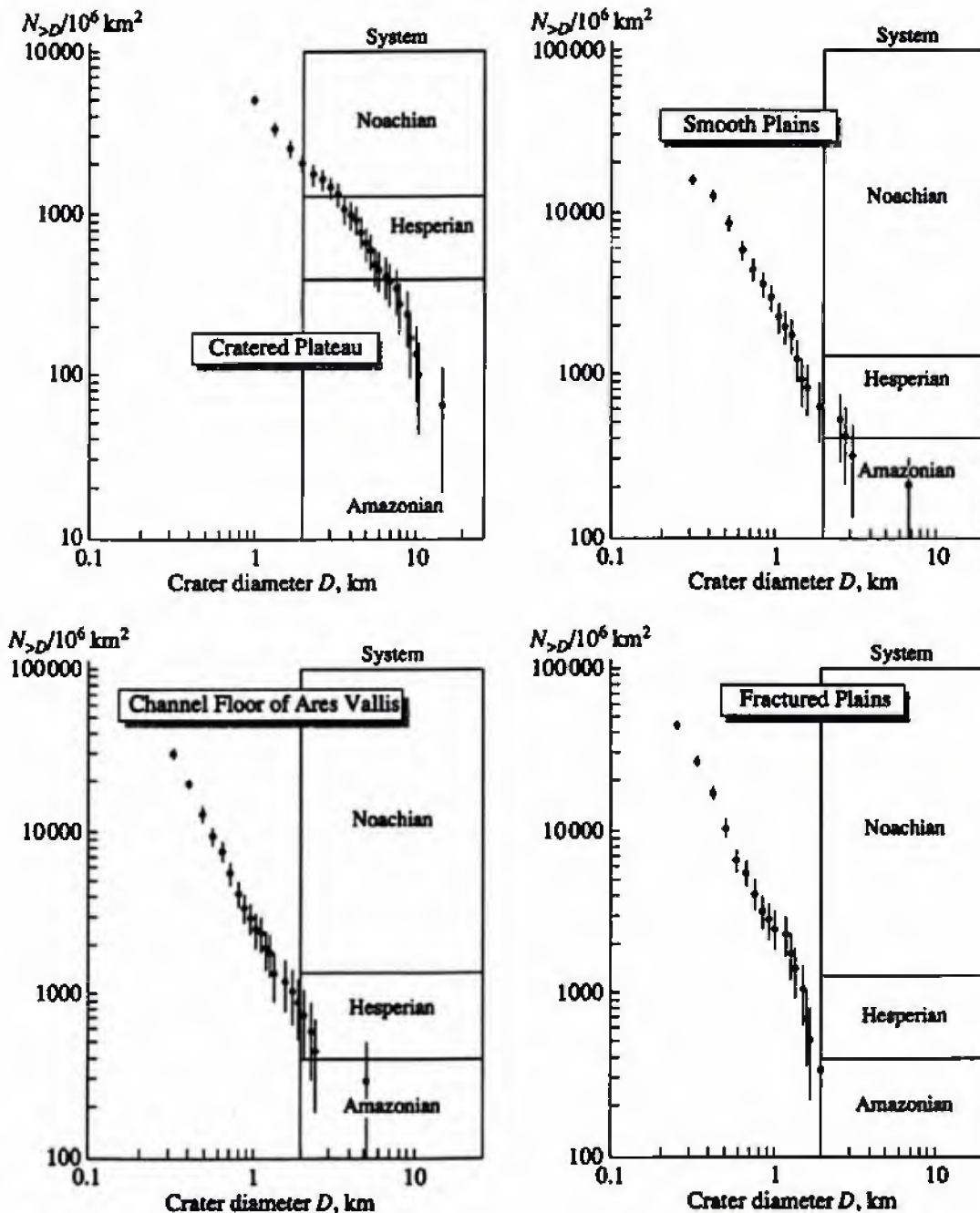
Fig. 3. Some results of the crater-density count for four different surface areas (only one distribution curve is shown for each unit). The Noachian, Hesperian, and Amazonian density ranges for craters greater than 2 km in diameter are from Scott and Tanaka (1986).

Tanaka (1997), who considers the ridged-plain material to be ancient and sedimentary in origin. This material could be transported from an ancient southern plateaux affected by intense Late Noachian erosion. In the north, it is overlain by younger deposits, and this situation was also noted by Scott and Tanaka (1986). In our stratigraphic scheme, we attribute this younger material to the lithologic units of smooth (SP) and spotted (StP) fluvial plains. In images of moderate resolution (e.g.,

633A41), the boundary between the older (RP) and younger (StP and SP) materials is undetectable. We think it corresponds to the boundary between the dark and bright areas in the low-resolution image 864A04 (Fig. 7). The Ares and Tiu valles are incised into the RP material, and the latter was thus eroded by the flows that have formed these valleys. Prior to the deep-incision state, the flows likely meandered over the RP surface producing faint channels and islands (FC). The

calculated density of impact craters suggests the Late Noachian–Early Hesperian age of the RP material.

2.3. Materials of the Ares and Tiu Valles

In this section, we describe the materials characterizing the floor, benches, islands, and deltaic deposits of the Ares and Tiu valles. According to the formation age, we divide the material units into ancient, middle, young, and diachronous. The latter were formed in the course of the whole fluvial history of the region.

Ancient fluvial material. This group includes spotted (StP) and smooth (SP) plains, and also faint fluvial channels and islands (FC).

Spotted plains (StP, Figs. 7 and 8) are relatively dark and display brighter splotches, whose diameters vary from a few kilometers to tens of kilometers. Within these plains, there are low ring rims, lacking ejecta zones. They seem to be the rims of impact craters partially overlain by the material of the plains. Lighter splotches may represent small islands of older material, most likely, of the ridged plains (RP) bordering the spotted plains (StP) in the south, or of the cratered plateau (CP). If the lighter areas are actually remnants of this type, then the dark plains in between represent the StP material itself. This combination of dark and lighter splotches may be indicative of a relief with depressions representing sags formed after thawing of the frozen ground or may be eolian in origin, as it is especially evident in the case of pitted plains (PP, see below).

The StP material is detected precisely in the mouth of the Ares and Tiu valles (Fig. 1b) and may be deltaic in origin. The spotted plains were eroded by the flows responsible for the carving of the Ares and Tiu valles (Fig. 7). Eastward of the Crater Wahoo (Fig. 8), the spotted plains (StP) are bordered by a steep slope or scarp facing the pitted planes (PP); in other words, the StP material is located higher in the relief than the surface of the latter. According to our photoclinometric measurements, the altitude difference between the StP and the PP surface level is less than 80 m. The scarp morphology suggests its erosional genesis.

The boundary between the spotted (StP) and the neighboring smooth plains (SP, see below) is vague. As semiburied craters are detected in both types of plains, we may assume a similar formation style under subaquatic conditions. The material of both may represent deposits of the intermediate (StP) and the distal (SP) part of the alluvial fans produced by catastrophic floods, as shown in the schematic published by Rice and Edgett (1997).

The unit of *smooth plains* (SP, Fig. 6) characterizes relatively dark smooth areas sculptured with rare wrinkle ridges. A relief of this type is detected in the northeast of the region. Young impact craters in the smooth plains (SP) are surrounded by a bright halo and rays, which presumably mark ejecta of a lower and older material lighter in color and representing, most proba-

Fig. 4. Cratered plateau (CP), hills (H), and ridged plains (RP) as seen in *Viking Orbiter* image 864A08 (north is at the top in all images).
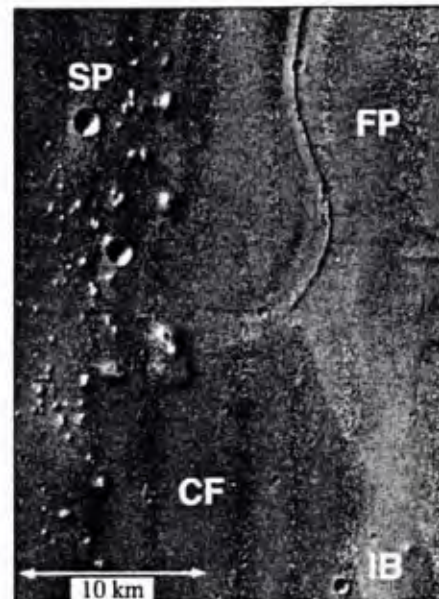

Fig. 5. Tiu Vallis floor (CTF), fractured (FP) and smooth (SP) plains as seen in *Viking Orbiter* image 669A91. Mudflow material from the fractured plains covers the valley floor, smooth plains, and the basal parts of some hills.
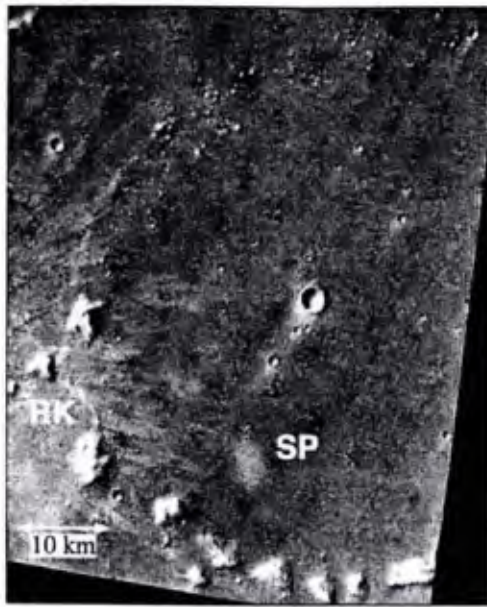
Fig. 6. Rings of knobs (RK) and smooth plains (SP) as seen in *Viking Orbiter* image 670A33. Greater sizes of the hills in the south may indicate either the northward-growing thickness of the overlying material of smooth plains or the intensification of ancient erosion in this direction. Bright rays around an impact crater located westward are seen at the left.
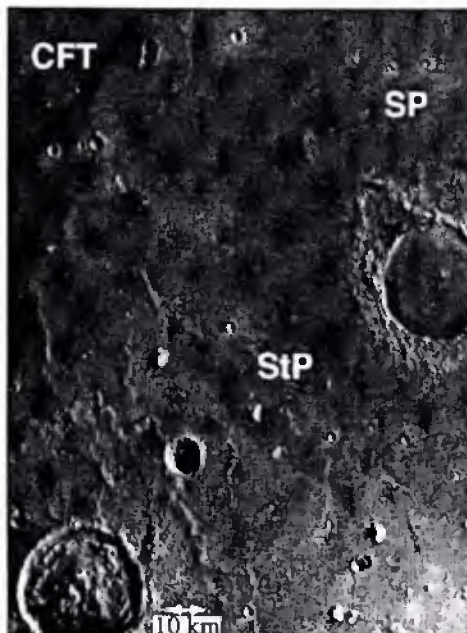

Fig. 7. Spotted (StP), smooth (SP), and ridged (RP) plains, as well as the Tiu Vallis floor as seen in *Viking Orbiter* image 864A04; Crater Libertad is in the left lower corner.

bly, the material of ridged plains (RP) or cratered plateaux (CP). Ancient craters are partially buried in the smooth plains (SP) by the material of the latter. Ruins of one very ancient crater are seen at 26° N, 26° E (Fig. 6) as a semicircle of knobs (RK material) that is open toward the north and suggests either a thickening of the overlying deposits in this direction, or the previous destruction of the northern sector of the crater rim. Within the smooth plains (SP), the smallest craters that are partially buried but still visible are about 3 km in diameter. Rims of these craters are 80–100 m high (Pike and Davis, 1984), and the layer of the SP material should be less than 80–100 m thick.

The smooth-plain material was previously considered volcanic (Scott and Tanaka, 1986) or sedimentary in origin (Rice and Edgett, 1997). In the studied region, we did not find any signs of its volcanic genesis, e.g., the outlines of lava flows or volcanic vents. The formation of these plains under subaquatic conditions (Parker *et al.*, 1989; Scott *et al.*, 1991; Tanaka, 1995) seems to be more realistic. Relations between this material and the Tiu Vallis floor (CTF, see below) suggest the erosional incision of the latter into the SP material (images 670A26 and 670A27), and we may state that the Tiu Vallis is younger than the smooth plains. The boundary between fractured (FP) and smooth plains is indistinct, but the material of the former is deposited over the Tiu Vallis floor, and they should be younger than the smooth plains. The cumulative-density plot of impact craters (Fig. 3) illustrates our data for one of five SP areas for which we performed crater counting. Judging from all the data obtained, the area in question is of the Late Hesperian age, whereas four other SP areas are of the Late Noachian–Early Hesperian age.

The unit of *faint channels and islands* (FC, Fig. 9) characterizes areas with indistinct furrows and elongated rises, which are about 10 km wide, and decorates the surface of the cratered plateau (CP) and of ridged (RP), smooth (SP), and spotted (StP) plains, where the material is similar in brightness but distinct in morphology. The FC materials are eroded by valley-forming flows and buried under the FP material (see below) and ejecta of the Libertad impact crater. The FC deposits may represent products of the initial stage of fluvial activity in the region, when water flows did not carve their certain waterways and flooded the plains widely (Nelson and Greeley, 1996, 1998).

Fluvial materials of intermediate age. The stratigraphic units in question are characteristic of the Ares Vallis floor (CFA) and of pitted plains (PP). We divided the CFA surface into plains of several morphological types (CF_{1-4}).

The Ares Vallis floor (CFA) is seen in the southern and central parts of the region. Some investigators, e.g., Rotto and Tanaka (1995), consider valley floors a morphological, rather than a geological, subdivision, ascribing to them solely the erosion genesis. On the Earth,

however, valleys of catastrophic water outflows host their own deposits (Rice and Edgett, 1997; Butvilovskii, 1993). In the mouth of the Ares and Tiu Valles, where the flow energy should be considerably decreased, the deposition of sediments is inevitable. The idea that catastrophic-flood deposits occur at the floor of the Ares and Tiu Valles and in their mouth is supported in addition by the results of the analysis of *Mars Pathfinder* panoramas (data on the size range of coarse clastic material; see Golombek *et al.*, 1997a).

Four morphological varieties of CFA plains are as follows: most widespread smooth plains with occasional furrows (CF_1, Fig. 10); hilly plains (CF_2, Fig. 11); plains with frequent, yardang-like ridges (CF_3, see image 003A57); and fretted plains (CF_4, Fig. 12). These morphological varieties of the Ares floor plains could be related in origin to differences in hydrodynamic conditions between different parts of the valley-forming flows, to variable environments of subsequent modification of the plains, to the substratum diversity, or to a combination of all these factors. In some works (e.g., Costard and Kargel, 1995; Kuzmin and Greeley, 1995a), the eolian deflation and thermokarst are supposed to be the main reworking mechanisms that have affected the valley floor after exsiccation and, possibly, is in progress now.

Plains CF_1 are smooth; they display rare longitudinal erosion grooves and hills resembling those of the H-unit—the classic type of outflow valley floor. Apparently, the hills were formed in the course of incision into older units under the influence of catastrophic flows of water (Baker, 1982). Their surface is locally covered with dark and bright streaks and spots with vague boundaries. These are likely traces of subsequent eolian redistribution of the material (see section 2.6).

Plains CF_2 are spotted by frequent hills, also resembling the H-hills and varying in diameter from hundreds of meters to a few kilometers. In this case, knobs may represent either mesas or huge rock blocks that were dragged by the valley-forming flows. According to estimates by Komatsu and Baker (1997), the catastrophic flows responsible for the origin of the Ares Vallis were able to drag blocks as large as 10–100 m across. As a rule, hills under consideration are larger and seem to be of erosional, rather than fluvial, genesis. According to Tanaka (1988), the hills in the mouth of the Tiu and the nearby Simud Vallis may represent, however, deposits of the debris flow.

Ridges of the yardang type are characteristic of the next plain category, CF_3. They are usually as wide as 100–200 m, occasionally up to 2 km, and as long as 30–40 km. Baker (1982) believes that some of the most elongated ridges in the Ares Vallis floor are true yardangs formed by eolation in a relatively soft fluvial material. Actually, ridges with the CF_3 morphology may exemplify these landforms; however, in our case, they are elongated parallel to the valley walls, i.e., discordantly relative to the bright and dark wind streaks

Fig. 8. Spotted (StP) and pitted (PP) plains as seen in *Viking Orbiter* image 034A89. A partially buried crater is located in the upper image area.

(Figs. 1d, 1e). Accordingly, their eolian genesis, at least under the current wind regime, seems doubtful. It is likely that these morphological areas of the Ares Vallis floor were created by fluvial incision into a material different from the rocks characteristic of the valley floor where other morphological varieties occur.

The surface of CF_4 plains is fretted, displaying an alternation of ridges and depressions of irregular shape. The ridges are from hundreds of meters to a few kilometers wide and up to 10–15 km long; the depressions are up to 10 km across. Rotto and Tanaka (1995) assume that areas of the CF_4 type are composed of a material resistant to fluvial erosion, whereas Costard and Kargel (1995) believe that the respective system of ridges and depressions is of thermokarst or eolian origin. In addition, Costard and Baker (1995) suggested the glaciofluvial genesis of this relief. It is also possible that the cauldron-type subsidence also contributed much to the formation and deepening of the Ares Vallis floor (Sharp and Malin, 1975). According to our measurements, the valley in the region is 600–1200 m deep.

The Ares Vallis is incised into the material of the cratered (CP) and knobby plateaux (KP), or into the ridged (RP) or spotted (StP) plains. Accordingly, we may assume that its incision down to the present level took place after the formation of ancient fluvial deposits (StP and SP). A catastrophic flood of that time could also be responsible for the Tiu Vallis formation, because both valleys have tributaries from the Hydaspis Chaos, which are approximately concurrent in age (Rotto and Tanaka, 1995). At present, however, the Tiu Vallis floor is incised into that of Ares Vallis and thus should be younger. The crater-counting results for the Ares Vallis floor suggest its Hesperian age.

Pitted plains (PP, Figs. 8 and 11) characterize relatively bright surface areas with abundant dark, flat-bottomed depressions approximately 30 m deep (Costard
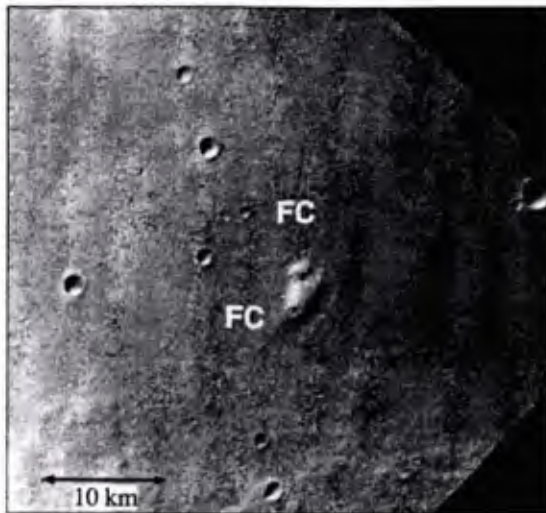
Fig. 9. Faint channels and islands (FC) inside smooth plains (SP) as seen in *Viking Orbiter* image 003A16. Fluidized ejecta from Crater Libertad are scattered in the right upper corner.

Fig. 10. Islands and benches (IB) in the Tiu Vallis as seen in *Viking Orbiter* image 003A14. The valley floor is smooth (CF₁).

and Kargel, 1995). Joining locally, these depressions form branching, gorge-like features opening into dark plains (DP, see below). In the western part of the region, pitted plains exhibit bench-like forms and islands located in the common mouth of the Ares and Tiu Valles (Fig. 1b). Treiman (1995, 1997) reported alternating bright and dark horizons in the scarps of bright

and other plains and plateaux located in the mouth of the Ares and Tiu Valles. Some researchers (Scott and Tanaka, 1986; Rotto and Tanaka, 1995) argued for the volcanic origin of this material; however, in morphology, the pitted plains better correspond to the karst areas of the Earth. Costard and Kargel (1995) believe that abundant thermokarst cauldrons in the pitted plains (PP) were formed over a ground saturated with ice, but they also do not exclude the possibility that these cauldrons are products of deflation. The material saturated with ice could be of fluvial, lacustrine, or glacial origin. Tanaka (1997) suggested that it was transported mainly from the Maja Vallis, located further westward. According to Kuz'min (1996), the unit under consideration characterizes the fluvial deltaic deposits of the Ares and Tiu Valles, and this viewpoint seems to be most reasonable.

Islands of the pitted plains (PP) extend southwestward to 20° N, 38° E, crossing the mouth of the Ares, Tiu, and Simud valles. Apparently, the deltaic sedimentation that deposited the PP material was spread over a vast area.

As mentioned above, the spotted plains (StP) are bordered by a scarp facing the pitted plains (PP). It is possible to suggest two models for scarp formation: either the mudflow forming Tiu Vallis reached the lower level of the PP material after the erosion of the StP material, or the PP material was deposited during the accumulation stage that followed the erosion period. In the latter case, the pitted plains (PP) are younger than ancient fluvial deposits and, being of fluvial origin as well, they characterize the subsequent stage of erosion and accumulation in the valley. The pitted plains (PP) were eroded by the Tiu Vallis flow, and, probably, the boundary between the Tiu Vallis and the Ares Vallis was simultaneously destroyed. The cratercount results suggest the Late Hesperian–Early Amazonian age for the pitted plains (PP).

Young fluvial materials. This group includes the Tiu floor (CTF) and dark plains (DP). Plains of several morphological types (CF₁₋₂ and CF₅) are distinguished in the CTF area.

The Tiu Vallis floor (CTF) is spread over a greater area of the studied region than that of the Ares Vallis floor. It exhibits two morphological varieties of plains characteristic of the latter: smooth, more spacious plains CF₁ and hilly plains CF₂. Plains of a new type, fretted at the surface and spotted with bright depressions (CF₅, Fig. 13), are also distinguished in the Tiu Vallis floor. These plains are spotted in images and display distinct bright depressions of irregular or elongated shape and also dim bright spots. The diameter of the depressions varies from hundreds of meters to 20 km. They are about 20 m deep (Golombek *et al.*, 1997b) and may represent a result of fluvial or eolian erosion that removed the dark upper horizon and exposed the underlying bright material. The latter may also correspond to younger eolian products accumu-

lated here (Komatsu *et al.*, 1995). Eolian sand is thought to represent also the material of the dark upper layer (Edgett and Christensen, 1994; Kuzmin and Greeley, 1995a, 1995b). In the opinion of Tanaka (1988), the material of these plains represents debris-flow deposits. Locally, the CF_5 plains incorporate mesa-type rises of bright material up to 5 km in diameter (images 006A19 and 003A20). One of them, decorated with a caldera-like depression, is less than 100 m high, according to our measurements. Rises of this type may be mesas of deltaic pitted plains (PP). An area of chaotic valley-like depressions is clearly seen within the CF_5 plain in images 006A17 and 006A34. These landforms presumably appeared as a result of the thawing of the permafrost zones. In some places of CF_5 plains, bright depressions are located close to teardrop-shaped islands and are elongated in the same direction, thus being formed by the same flows (images 003A50 and 004A17). Other bright lineaments, which may mark scarps or fractures, are discordant relative to the flow direction (images 004A16 and 004A79). Thus, the origin of CF_5 plains is not yet clear. They might be the result of the particularities of fluvial erosion that operated in these areas, and from subsequent thermokarst and eolian reworking.

The Tiu Vallis is incised into the Ares Vallis floor, as well as in several other units, such as knobby plateaus (KP) and plains of the ridged (RP), spotted (StP), smooth (SP), and bright (PP) types. The fractured-plain material (FP, see below) lies over the Tiu Vallis floor (CTF, Fig. 5). According to the crater-counting results, the Tiu Vallis floor is Late Hesperian–Early Amazonian in age (Fig. 3).

Dark plains (DP, image 24A55) are located downstream of a bench composed of pitted-plain (PP) material. It is possible that these plains (DP) represent only a part of vast fluvial plains located in the mouth of the Tiu and Simud Valles. Morphological varieties CF_1 and CF_2 of the Ares Vallis floor (see above) are also characteristic of the dark plains (DP). As the surface of the latter is darker than the Tiu Vallis floor at the same latitude, it appears to be covered with a dark eolian material (in general, the further north, the darker the surface of the region). This situation is also seen in the Wahoo Crater adjacent on the east and displaying a dark floor (in the region at hand, dark streaks are situated east of the craters; see section 2.6). The northern dark plains seem to be incised into the material of spotted and smooth plains; they are overlain, in turn, by the material of fractured plains (image 008A51) and are older than it.

Diachronous fluvial islands and benches (IB, Fig. 11). *Fluvial islands and benches* everywhere are in contact with the valley-floor materials. South of 25° N, the slopes of islands and benches are steep or stepwise (morphological variety IB_1). Near 20° N, 30.5° W, Kuzmin and Greeley (1995a, 1995b) detected eight slope steps, and near 23° N, 30° W, we distinguish four steps. Northward of 25° N, the slopes of islands and
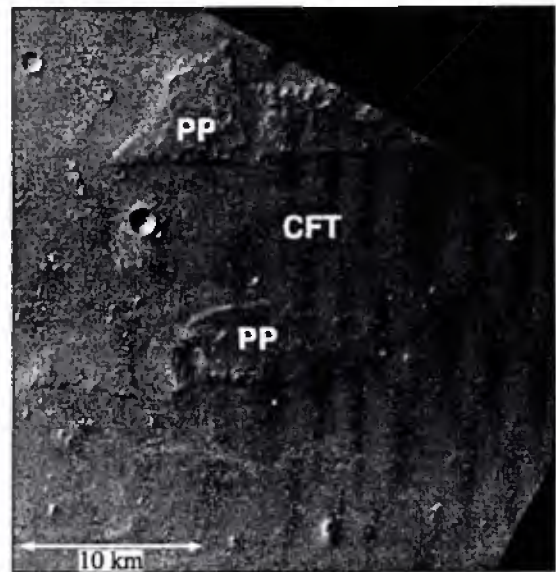

Fig. 11. Erosion remnants (islands) composed of the pitted-plain material (PP) as seen in *Viking Orbiter* image 003A24. The valley floor is decorated with many hills (CF_2).

Fig. 12. Fractured monotonous valley floor (CF_4) as seen in *Viking Orbiter* image 864A12.

benches become less steep and steps are lacking (image 670A16, morphological variety IB_2).

Features of the IB_1 type appear to be formed by the incision of valley-forming flows (Baker, 1982). Two mechanisms for step formation were suggested. First (Kuzmin and Greeley, 1995a, 1995b), this may be a result of the erosion of layered deposits left by previous flood events and partially duricrusted (Treiman, 1995,

Fig. 13. Fractured valley floor with bright cauldrons (CF$_5$) as seen in *Viking Orbiter* image 004A62.
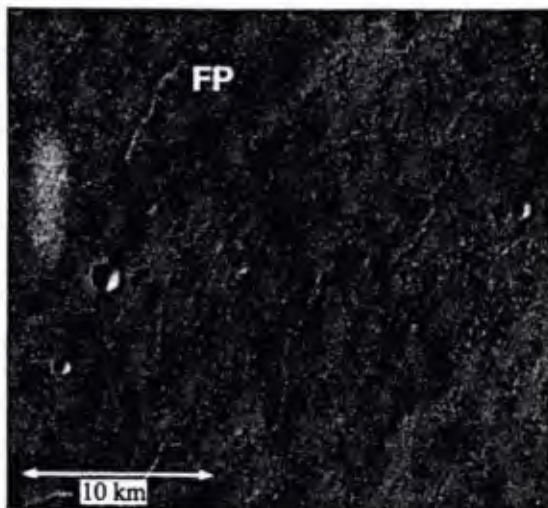

Fig. 14. Fractured plains (FP) with conformably striking ridges and fractures as seen in *Viking Orbiter* image 632A12.

1997). Second, they may reflect the pulsating incision of flows (De Hon, 1989) into a homogeneous, nonlayered ground.

We measured the hypsometric parameters of two typical islands crowned with the Bok and Gold craters and of a small island situated in between. The slopes are stepwise at the rear side of the islands and steep at their front side, where the top surface is bordered by escarpments. The flat top surface of the islands is elevated 30–60 m above the nearby plains. Baker (1982)

believes that the escarpments are characteristic of those island tops which were partially affected by the last flood event.

As for the northern islands and benches displaying smooth, gentle slopes (morphological variety IB$_2$), they could be formed in the zone of accumulation and weak erosion in the valley mouth. According to Baker (1982), their gentle slopes mean that the islands were completely flooded during the last stage of fluvial activity.

It is also likely that islands and benches were taking shape during all episodes of catastrophic floods, when flows incised into the material of plains and plateaux. In this case, their material represents a mixture of eroded rocks and sediments deposited by the flows. Benches of the IB type are inset into ridged (RP), spotted (StP), bright (PP), and, possibly, smooth (SP) plains. The material of fractured plains (FP) locally overlies the basal horizons of the northernmost islands (image 669A93), thus being younger than the IB unit.

2.4. Fractured Plains (FP) Postdating Valley Formation

Fractured plains characterize areas displaying narrow fractures, trenches, and ridges in their central parts (Figs. 5 and 14). Fractures and ridges are about a half-kilometer wide, whereas trenches are up to 2–4 km across. The length of these features ranges from a few to 40–50 km. Inside the fractured plains (FP), hills comparable in size with those of the H-type are surrounded by benches. Ridges and fractures are often oriented conformably (Fig. 14), or the latter may cross the former. In addition, some fractures cross ejecta of a young impact crater (Fig. 15), whose age is estimated to be 1.5 Gyr on the basis of counting results for smaller impact craters at its surface. Benches around the hills were classed with either wave-abrasion platforms (Parker *et al.*, 1993), or slope-subsidence forms (Lucchitta, 1984). The observed orientation of fractures and ridges, longitudinal to transverse relative to the valleys, suggests they might be formed in the course of exsiccation, sagging, and freezing–thawing cycles, which occurred in combination or separately in the water-saturated material (Jöns, 1986; McGill and Knobs, 1992; Parker *et al.*, 1993). Ridges may represent a result of the water-rich material squeezing from below, when the upper layer was already frozen (Tanaka, 1997). Lucchitta *et al.*, (1986) argue for a certain similarity between these forms and some ridges of the Antarctic shelf and suspect they originated under subglacial environments. Other scientists argue for coastal and fluvial origins of the ridges (Parker *et al.*, 1993; Scott, 1982).

Between the FP and valley-floor materials, there are frequent lobate flows, whose orientation suggests that they penetrated into the Ares and Tiu Valles from the north. Jöns (1984, 1985, 1986) related them in origin to the material incursions from a hypothetical mud ocean that existed, according to his opinion, in the northern

plains. Tanaka (1995, 1997) suggested that this material (like that of the valley floors) was transported from the plains by catastrophic floods, whose frontal parts rose up the slopes by inertia and then rushed back. Parker *et al.*, (1993) interpreted these lobate flows as analogues of terrestrial alluvial fans of subaquatic mudflows. Under Martian conditions, these features could be produced when flows saturated with a clastic material rushed into an ancient sea or ocean.

Thus, the FP material is of unclear origin. In our opinion, it is sedimentary and originally was saturated with water or ice (Lucchitta *et al.*, 1986; Tanaka, 1995). According to crater-counting results, this material is of the Late Hesperian–Early Amazonian age. The FP material was formed either at the stage of fluvial activity that deposited the Tiu floor sediments, or, more likely, later, when a catastrophic flood event brought the material from another valley located somewhere nearby. Only the eolian deposits and fresh impact craters are younger than the FP material.

2.5. Materials of Impact Craters

Impact craters (Fig. 7) formed during the whole geological history of the region. In the map (Fig. 1b), we depicted 76 craters with diameters greater than 4–5 km; 17 of them are more than 16 km across, and 4 are more than 40 km across (the largest, the Kipini Crater, is 70 km in diameter). Some craters are relatively fresh; others, heavily destroyed. The former dominate among smaller craters, whereas larger ones are frequently ruined. We divided the crater materials into the *ancient-crater complex* (ICo), *rim-and-floor complex of young craters* (IC), and complexes of *dry* (ICd) and *fluidized* (ICf) ejecta. Craters with fluidized ejecta indicating the presence of solid H_2O and other volatiles in the substratum (Carr *et al.*, 1977) are detected almost everywhere. Costard (1994) counted the number of craters with fluidized ejecta per $5° \times 5°$ cell for a vast area covering our region together with others. According to his evaluation, craters of this type represent from 13 to 53% of the crater population in a cell.

Figure 2 shows the stratigraphic position of two large craters: Libertad (IC and ICf subunits) and Wahoo (ICo unit). Ejecta from the Libertad Crater overlie the FC, SP, and StP deposits, whereas the younger Tiu Vallis is incised into these ejecta. Consequently, the impact event was intermediate in time between the first and the last stage of fluvial activity. The same situation is characteristic of a nameless adjacent crater located northeast: its ejecta rest on the FC material, being overlain, in turn, by ejecta from the Libertad Crater. The Wahoo Crater apparently escaped the Late Noachian stage of intense denudation. Its ejecta underlie ancient fluvial deposits (SP and StP), and the crater formation thus predates the accumulation period of the latter. The Soochow and Zuni craters (IC and ICf subunits) are superposed onto the ridged plains (RP) and seem to have been formed after them, but prior to the termina-

Fig. 15. Fractured plains (FP) as seen in *Viking Orbiter* image 669A69. A fresh impact crater is located in the lower right corner and a young fracture in the center cuts the ejecta from this crater.

tion of erosion in the Ares Vallis, because they are eroded. The Concord and Ore craters (IC and ICf subunits) may have been formed between two stages of fluvial activity in the Ares and Tiu Valles, since they are located on the erosion surface of benches, and in turn, were eroded by valley-forming flows.

In addition to primary impact craters, we detected small secondary craters in the region, which appeared after impacts of ejecta from the primary impact structures. The secondary craters are concentrated in the meridional zone between 18°–24° N and 31°–33° W. Kuz'min (1996) believes that they were produced by ejecta from the 50-km-wide crater distinct in morphology and located at 7.5° N, 32.9° W.

2.6. Eolian Materials

Eolian materials (Figs. 1d and 1e) are the constituents of several features of the Martian surface, such as: *bright wind streaks* (Wsb), which extend southwestward and range from a few to 100 km wide and from a few to 50 km long, depending on the size of the screen behind which they accumulated; *dark areas* (Wsd), which are from a few to 200 km across and represent wind streaks extending from west to east and in the west-southwestern direction, and also dark deposits on the floors of valleys and of the largest impact craters, in their southwestern sectors; and *bright to dark, narrow wind streaks* (Wsn, image 524A26), which are variably oriented and up to a few tens of kilometers long and wide. The last features may indicate a diversity of wind
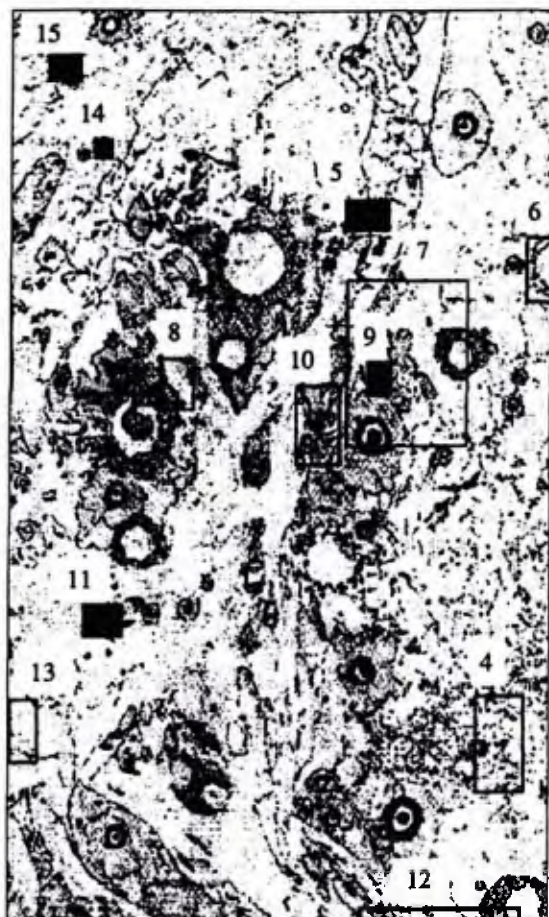
Fig. 16. Mosaic of images shown in Figs. 4–15.

directions, as they were formed in different epochs. In the region considered, we also detected two areas where elongated ridges resembling yardangs are up to a few kilometers long and extend either south-south-west (the Wahoo Crater floor, image 34A90) or west-southwest (ejecta of the Kipini Crater, image 669A86). In our opinion, these are purely erosional, but not litho-logic, formations.

The dark eolian material most likely corresponds to sand that was derived from the Acidalia Planitia and covered the valley floors (Edgett and Christensen, 1994; Kuzmin and Greeley, 1995a). If this assumption is correct, the abundance of sand may grow northward. Actually, the color images of the region show that, in contrast to southern areas, all materials located north of 20° N, with the exception of a few crater rims and bright streaks, are dark and bluish at the surface, which is characteristic of eolian sand (see below).

The low resolution of images did not allow us to detect eolian dunes in the region, where they might be widespread. Small dunes were pictured directly at the *Mars Pathfinder* landing site (Matijevic *et al.*, 1997). Many dark spots inside craters may also correspond to sandy dunes (Arvidson, 1974). Rice and Edgett (1997)

believe that the entire northern part of the region (the distribution area of FP and SP materials) is covered with sandy deposits of catastrophic outflows, which have experienced eolian reworking and incorporate small, isolated dunes. The elongated dark splotches in the low-resolution images presumably mark dune clus-ters located north of 27° N, within the spotted and frac-tured plans. Wind streaks formed by barchans, which are well known on the Earth and on Mars, may also occur in the region under consideration.

In the stratigraphic aspect, the eolian materials are younger than the surface they overlie.

2.7. Stratigraphic and Age Relations between the Units

The revealed stratigraphic succession of material units and respective landforms can be used as an indi-cator of principal stages in the geological history of the region. The first events at the surface of the ancient highland were the destruction of the cratered plateau (CP) and the formation of the ridged plains (RP). Ejecta from the large Zuni and Soochow impact craters overlie the ridged plains but are eroded by flows that created the Ares Vallis, and this indicates that the timespan between the ridged-plain formation and the next resur-facing stage was significant, because great impact events are fairly rare. Our data, and those of others (Kuzmin and Greeley, 1995a, 1995b; Nelson and Gree-ley, 1996, 1998; Rotto and Tanaka, 1995; Tanaka, 1995), suggest that catastrophic floods in the Ares/Tiu mouth were recurrent. In our opinion, this is evident, first of all, from several generations of fluvial deposits and landforms, which are incised into one another, suc-cessively overlie one another, and were, therefore, formed at different stages of erosion and accumulation. Faint fluvial channels and islands (FC) along with spot-ted (StP) and smooth (SP) plains originated first, prior to the appearance of major valleys. The stratigraphic position of the Libertad and another nameless crater located nearby (see above) shows that both impact events took place between the first and the third outflow and, consequently, these outflows were separated by a considerable time interval. The second outflow (possi-bly a simple continuation of the first one) was respon-sible for the erosion of older deposits, created the Ares floor surface (CFA), and deposited the material of the pitted plains (PP). The escarpment between the spotted and pitted plains might be formed by the incision of the valley into its own deposits. The third outflow from the Tiu Vallis eroded these deposits and the Ares Vallis floor; however, it is difficult to determine the length of time between this and the second outflow. Anyway, the hypothesis of two catastrophic flood events separated in time seems to be quite reasonable. The fractured plain material (FP) lies over the young fluvial deposits of the Tiu Vallis floor (CTF) and dark plains (DP), being prob-ably even younger.

In summary, we may suggest the following sequence of geological events in the region: the forma-

tion of the cratered-plateau material (CP) —→ its erosion and the partial accumulation of the ridged-plain material (RP) above the plateau —→ the first catastrophic flood, which left behind the material of small islands and valleys (CF) and the deltaic deposits of smooth (SP) and spotted (StP) plains —→ the second flood, which deposited the material of the Ares Vallis floor (CFA) and pitted plains (PP) —→ the third flood and the formation of the Tiu floor deposits (CTF) —→ the appearance of the fractured-plain material (FP). Eolian processes and impact cratering at the Martian surface have apparently lasted throughout the geological history of the region.

3. SURFACE CHARACTERISTICS INFERRED FROM IMAGES OBTAINED WITH DIFFERENT FILTERS AND FROM THERMAL-INERTIA DATA

3.1. Surface Color

It is well known that various regions of the Martian surface are colored dark-gray or bright- to dark-red, presumably depending on the local composition of the surface material (Arvidson et al., 1989; Mustard, 1995). As assumed, the dark-gray areas mark either relatively fresh outcrops of mafic rocks and sand or very thin, palagonite-like dust covers overlying them. The bright-red areas are assumed to be covered with oxidized palagonite-like material, including eolian dust. The dark-red surface is thought to characterize a mixture of a dark-gray and a bright-red material or to consist of immature weathering products formed over a basaltic basement (Mustard, 1995).

In order to reveal the characteristics of distinguished material units, we studied images obtained with different filters, analyzing the brightness ratio between the red and violet spectral ranges and correlating this parameter with a thermal-inertia map (Christensen and Kieffer, 1989). The same approach was used by Soderblom et al., (1978) and Arvidson et al., (1982), who studied other areas.

The original images of the same area (Soderblom et al., 1978) were made by the *Viking Orbiter* with three filters: violet (0.45 ± 0.03 µm, image 666A52), green (0.53 ± 0.05 µm, image 666A56), and red (0.59 µm, image 666A58). These images allowed us to characterize most units distinguished by us, although their resolution is low, only 0.82 km per pixel. The brightness-distribution histogram for the red spectral range shows two distinct peaks, one corresponding to surface areas located north of 20° N and another, south of this latitude. This may indicate that materials in the two parts of the region are different in composition. In order to analyze the images in greater detail, we selected 48 small areas in which the surface color of one or another unit is approximately the same over a mosaic of the red, green, and violet images superimposed. Some units with varying surface color were studied in their several areas. For instance, we investigated five areas of

the Tiu Vallis floor notably contrasting in color one to another. For each of the studied areas, we measured the radiance factors in all the three spectral ranges, reconstructed their spectra, and determined the radiance ratio between the red and the violet spectral range using a technique described by Arvidson et al., (1982).

In the plot illustrating the variation of the red-range radiance factor versus the red-to-violet brightness ratio (Fig. 17), one can distinguish several color groups of materials. The darkest blue material is characteristic of deposits in the impact craters and northern areas of the valley floors. This material most likely corresponds to eolian deposits, and the dark color suggests that they are mafic in composition. The bright-red color is typical of wind streaks and plateaux located in the south and may characterize eolian dust. The dark-red areas in the south of the Ares and Tiu Valles and in the neighboring plateaux may indicate a duricrusted soil or a mixture of dark and bright materials (Arvidson et al., 1989; Mustard, 1995). In Fig. 17, the material that is in an intermediate position between these groups of materials may characterize a surface composed of two or three components. Three principal color groups are perfectly distinct in the plot of three-component spectra (Fig. 18). In the violet spectral range, their radiance factors are almost identical, whereas the dark-gray material is least bright in the green and the red range. The bright- and dark-red materials are also different in these spectral bands.

Our analysis also revealed that the rims of ancient impact craters are colored brighter in red than surrounding areas, as was first noted by Soderblom et al., (1978).

3.2 Thermal-Inertia Data

The thermal-inertia parameters of the ground may be used for the evaluation of the material-grain size (Edgett and Christensen, 1997). Our analysis of these parameters was based on the thermal-inertia maps published by Christensen and Kieffer (1989) and Edgett and Christensen (1997). In the first map, the thermal inertia is represented by contours with an interval of 10^{-3} cal/(cm^2 s$^{0.5}$ K), and in the second, as discrete values with a resolution of 0.5° of latitude and longitude. In the region studied, the magnitude of thermal inertia, by and large, increase from south to north. Accordingly, on the basis of correlation between these values and the grain size of the material (Edgett and Christensen, 1994), we may assume that medium-grained sand is dominant in the south, whereas coarse sand is widespread in the north. However, this general trend is irrelevant in two situations.

(1) In the south, the thermal-inertia magnitude in the Ares Vallis ground is greater than in the nearby plateaux (CP and KP) and plains (RP). This indicates that the valley floor is covered with coarse or very coarse sand, whereas medium- to coarse-grained sands are widespread in plains surrounding the incised valley.
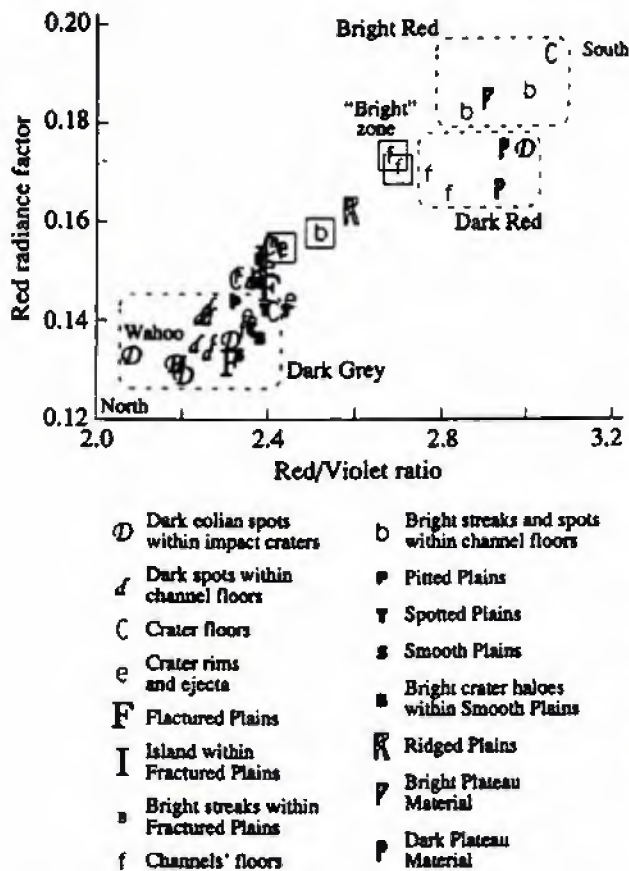
This situation, noted first by Betts and Murray (1993), may reflect either the originally coarser grain size of fluvial deposits or be a consequence of deflation that was most active in the valley and removed the fine-grained material from the fluvial sediments.

(2) Spotted (StP), dark (DP), and bright (PP) plains located approximately in the center of the region display abnormally high thermal-inertia magnitudes of $(12–15) \times 10^{-3}$ cal/(cm^2 s$^{0.5}$ K), characteristic of coarse sand or gravel (Edgett and Christensen, 1994). It is possible that fine particles were removed from the surface of these plains, or they were originally composed of materials with these granulometric parameters. On the Earth, such coarse deposits are characteristic, for example, of midfan facies of catastrophic flows (Rice and Edgett, 1997).

As for eolian deposits, which seem to be present in the region, they have no indications in the thermal-inertia map by Edgett and Christensen (1997). Possible explanations for this fact are as follows: the thermal mapping was of insufficient resolution; the bright dust covers are thinner than the layer, a few centimeters thick, affected by diurnal thermal fluctuations in the ground (Arvidson *et al.*, 1989); or the grain-size differ-

ence between eolian and surrounding deposits is insignificant.

3.3. Rock Abundance

Using the thermal-mapping data by the *Viking Orbiter*, Christensen (1982, 1986) estimated the relative abundance of rock fragments greater than 10 cm across occurring on the surface. His results are represented in a digital map with a resolution of 1° in latitude and longitude, which comprises the region of our study. In the region, this material is distributed irregularly: rock fragments occupy 0–5 to 21–25% of a given resolution element. Rocks are quite abundant in the spotted (StP), bright (PP), and dark (DP) plains. Their estimated abundance is decreased inside the two largest dark areas of eolian (WSd) material (29° N, 34° W and 28.5° N, 28.5° W; Figs. 1d, 1e); in a dark streak located at 26° N, 35.5° W; and in floor areas of the Kipini, Libertad, and the nameless crater situated at 15° N, 27° W. Within frequent narrow, bright streaks, rock fragments are locally more abundant (16–25%), and these areas seem to be heavily affected by deflation. Broad, bright streaks show a variable density of rock-fragment populations and are interpreted as areas of a weak deflation and dust accumulation, which do not affect this density. A moderate to low abundance of rock fragments is characteristic of cratered (CP) and knobby (KP) plateaux and of ridged plains (RP).

3.4. A Comparison of the Surface Color, Thermal-Inertia Data, and Rock Abundance

A comparison of these parameters allows us to distinguish three types of areas in the region: gray to dark-gray areas with high thermal-inertia magnitudes and variable amount of rock fragments; red to dark-red areas marked by low to moderate thermal-inertia magnitudes and irregular distribution of rock fragments; and red areas displaying high thermal-inertia magnitudes and abundance in rock fragments.

Gray to dark-gray material of the surface corresponds to the coarse sand and gravel (Fig. 19) and associated rock fragments distributed unevenly. According to their morphology, these dark streaks and splotches are attributed to sand-accumulation areas. It is also likely that dark eolian deposits in the Libertad, Wahoo, and Kipini craters predominantly consist of sand, because the estimated rock abundance here is a minimum. Sandy eolian deposits of mafic composition may also be typical of dark splotches in the valley floors and in the fractured (FP) and smooth (SP) plains.

Red to dark-red material with varying abundance of rock fragments may be considered a variable-proportion mixture of dust, sand, rock fragments, and duricrusted soil. The plateau areas where the thermal-inertia magnitude and rock abundance are at a minimum, are apparently covered with dust, possibly duricrusted. The bright wind streaks in the north are redder than in the

floor of the Tiu Vallis and fractured plains (FP), inside which they are located. However, thermal inertia anomalies are not typical of these features, and their sedimentary cover may be very thin (Arvidson *et al.*, 1989).

Dark and pitted plains with abnormally high thermal-inertia magnitudes, abundant in rock fragments (symbols f and P in Fig. 19), have red-to-violet brightness ratios close to the average value for the region at hand. This combination of parameters suggests that the material of these plains is most likely the same in composition as that of the floors of the adjacent valleys and fractured plains, but is coarser. Some researchers (Rotto and Tanaka, 1995; Nelson and Greeley, 1998) believe that the pitted plains (PP) and fretted plains in the south of the Ares Vallis floor (type CF_4 in our map) represent the same material unit. At the surface, however, their material is different in color and rock abundance, and their thermal-inertia parameters are also diverse.

Between 17° and 20° N, the floor of the Ares and Tiu Valles is similar in parameters to the dark-red surface ("bright" areas in Figs. 17 and 19). The *Mars Pathfinder* rover detected rock fragments, dust, and presumably duricrusted soil here (Matijevic *et al.*, 1997), which seem to be characteristic of the indicated area.

4. IMPACT-CRATER COUNTING

The cumulative spatial crater density was calculated for 12 areas of the region (Fig. 20, table). For the images available, our objective was to calculate the crater density in as many stratigraphic units as possible and to verify the results recurrently for units occupying large areas. Any of the 12 selected areas includes several stratigraphic units, and we calculated the crater density for each of them separately. Moderate-resolution images (36–52 m per pixel, 47 images in total) characterize 11 areas, and one more area was studied using low-resolution images (164 m per pixel, 7 images). The total area covered by counting was 230000 km^2. The smallest of the craters counted was equal to six pixels (216–984 m) in diameter. Some crater-counting results are illustrated in Fig. 3.

In order to evaluate ages relative to the major—Noachian, Hesperian, and Amazonian—epochs of the Martian stratigraphic scale, we used the data of Scott and Tanaka (1986), who counted craters greater than 2 km in diameter; the same condition for counting was applied in our case. The calculations yielded the Noachian age for the cratered plateaux (CP) and the Hesperian age for the Ares Vallis floor (CFA). Unfortunately, calculation errors are very high for subdivisions occupying small areas. In some of them, mainly, in smooth (SP) and fractured (FP) plains, the cumulative crater density varies considerably from one area to another. Accordingly, stratigraphic ranges are defined as Late Noachian–Early Hesperian for smooth plains and as
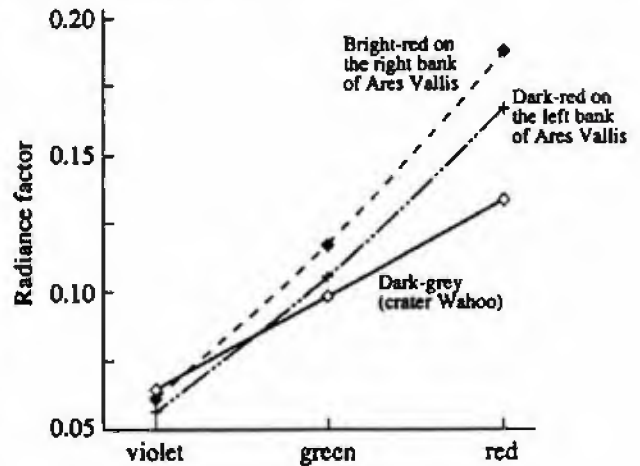

Fig. 18. Three-component spectra for surface materials most contrasting in color.

Hesperian–Early Amazonian for fractured plains. Such uncertainties may be due to the effect of subsequent resurfacing in a given area, the partial preservation of older crater populations, and the mere stochastic variations in the crater density.

In most cases, the areas of distinguished units are too small, and the number of craters exceeding 2 km in diameter is insufficient to reliably define the unit position in the Martian stratigraphic scale. To better understand age relations in this case, we compared the counting results for craters greater than 1 km in diameter (they are detectable in all stratigraphic units) between different units and then verified these relations, based on statistical results with age relations obtained from a stratigraphic analysis. This approach is used below to elucidate the principal resurfacing stages in the region.

5. PRINCIPAL RESURFACING STAGES IN THE REGION

The age succession of stratigraphic units distinguished and mapped in the region was used as a basis to depict the most significant resurfacing stages. This succession is substantiated by the revealed stratigraphic relations between surface materials and, independently, by the results of the impact-crater counting. Final results of this combined approach are shown in Fig. 21.

At the left of Fig 21, we plotted the crater-counting results for all stratigraphic units except the relic hills (H), rings of knobs (RK), and faint fluvial channels and islands (FC), the areas of which are too small and display an insufficient number of craters. This plot also demonstrates our counting results for two complexes of cratered (NPL_1) and eroded (NPL_2) plateaux distinguished by Rotto and Tanaka (1995) outside the area of our map. The crater density for old cratered plateaux (CP) or knobby plateaux (KP) may be underestimated
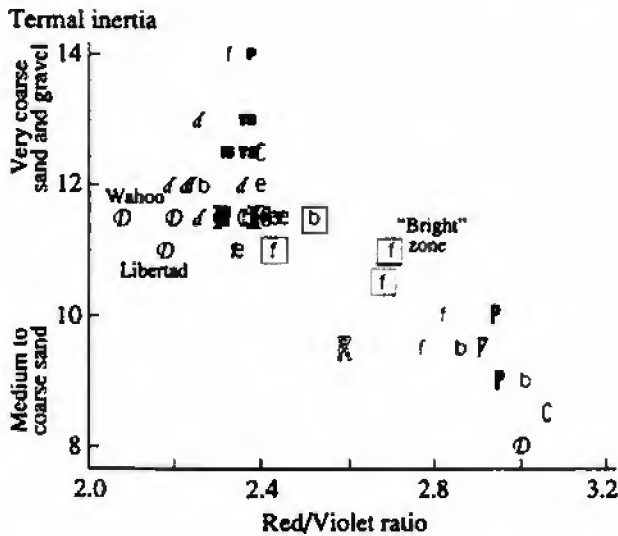
Termal inertia

Fig. 19. Variations in the thermal-inertia magnitudes [in units 10^{-3} cal/(cm^2 s$^{0.5}$ K); after Christensen and Kieffer (1989)] versus red-to-violet brightness ratios for different areas of the surface (symbols as in Fig. 17; indicated rock types from Edgett and Christensen, 1994).

because of the preferential destruction of small craters within these long-existing complexes.

Along the abscissa axis, units are arranged in their stratigraphic succession (Fig. 2) and divided into three groups (from left to right): (1) rims and ejecta of large impact craters; (2) fluvial deposits (StP, SP, PP, IB, CFA, CFT, DP) and fractured plains (FP); and (3) valley-predating units (NPL$_1$, NPL$_2$, CP, KP, RP).

At the right of Fig. 21, the relative age sequence of subdivisions also corresponds to that shown in Fig. 2.

The revealed stratigraphic relations between the units suggest that the main stages of the Martian surface reworking were the erosion in cratered plateaux and three catastrophic floods in the valleys (see above). The stratigraphic relations cannot elucidate, however, how long the timespans between these stages were. At the same time, using the crater-counting data, we may evaluate the intervals separating different geologic events (the sequence of which is suggested by the succession of material units; see the right side of the plot) in terms of impact-crater densities accumulated on a given area after its last resurfacing (left side of the plot). This evaluation is possible, of course, only if the intervals were sufficiently long to ensure a statistically meaningful difference between the densities of crater populations. In Fig 21, the stages of resurfacing inferred from stratigraphic relations and expressed in units of the cumulative crater density are marked by gray horizontal bands. The age position of stages (their interval in the scaled left ordinate) is estimated as described below.

Stage I: Erosion of the Cratered Plateau (CP) and Formation of Ridged Plains (RP)

Judging from the stratigraphic relations between the cratered plateaux and ridged plains, the former are older than the latter. Consequently, the band marking this stage should be placed above the crater-density value for the plateau (with due account for errors) but below the value characterizing the ridged plains. In view of a high error in one of two values estimated for the ridged plains, the crater density for the first band is assumed to be equal to that within the overlapping range of two estimates obtained for ridged plains (approximately 3300–4200 craters greater than 1 km in diameter per 10^6 km^2).

Stage II: Fluvial Reworking Postdating the Ridged Plains but Predating the Incision of the Ares and Tiu Valles

The stratigraphic relations (the right part of Fig. 21) show that the oldest fluvial deposits of the region that created the spotted (StP) and smooth (SP) plains were accumulated after the ridged-plain formation. The formation of islands and benches (IB) in the Ares and Tiu Valles floors presumably commenced at the same time. Accordingly, the horizontal band (second from below) marking the second stage of resurfacing and the first stage of valley incision is placed at the level corresponding to the overlapping range of crater-density values for ancient fluvial plains (StP and SP) but above the value characteristic of ridged plains (RP), i.e., within the interval of 2700–3300 craters greater than 1 km in diameter per 10^6 km^2. In this case, one of the SP and one of the IB area remain below this interval. Judging from the abundance of partially buried and eroded craters in these areas, this departure in the plot may indicate that they incorporate craters originated on an older surface (CP, KP, or RP). Another SP area plots above the indicated density band. However, it is located near the vague boundary with the younger FP surface and may thus belong to it. The time interval between the first and the second stage is probably short. We show it tentatively, without attributing any age significance to its width.

Stage III: The Incision of the Ares Vallis and Accumulation of PP material

Our stratigraphic analysis indicates that the Ares Vallis is incised into ancient fluvial deposits (SP, StP, FC). The deposits of pitted plains (PP) might be formed at the same time, although the PP surface could be heavily eroded by younger flows, which destroyed some craters and "rejuvenated" the surface. Accordingly, the horizontal band marking the age position of this stage is plotted at the level of the CFA unit above the previous stage (the range of 2200–2700 craters greater than 1 km in diameter per 10^6 km^2). Apparently,

the time gap between the second and the third stage was also not long.

Stage IV: The Tiu Vallis Incision

The crater-density band for this stage is bordered by the overlapping level of the values estimated for the CTF and DP fluvial materials deposited after the formation of the CFA and PP surface areas. In addition, this band should be placed below the crater-density values for the fractured plains (FP), whose material overlies the CTF and DP areas, i.e., within the range of 1300–1400 craters greater than 1 km in diameter per 10^6 km^2. We do not reject the fact that all three groups of material insignificantly differ in age. One area of fractured plains (FP) turns out to be below this band, because, as we think, some ancient craters remained unburied here by a thin sedimentary cover characteristic of this area. This situation explains why the crater-density values are greater here and the area looks older than other surface areas reworked at the last stage.

We should also add that all stages of impact cratering were paralleled by eolian processes, as at the present.

Thus, the combined analysis of stratigraphic relations, together with the results of impact-crater counting (Fig. 21), reveals four principal stages in the evolution of the Martian surface in the Ares–Tiu mouth. Three of them might be separated by perceptible timespans. These are stages I and III, separated by impact events that formed the Zuni and Soochow craters; stages II and IV, limiting the formation interval of the Libertad and the nameless crater; and stages III and IV, because the surface of their materials is characterized by notably different values of cumulative crater density.

Fig. 20. Areas selected for impact-crater counting (numbered as in the table).

6. AGE ESTIMATES FOR STRATIGRAPHIC UNITS AND RESURFACING STAGES

The absolute ages of the distinguished stratigraphic units were estimated by means of calibrating the crater-counting results with the use of the reference curve of crater density versus the crater-accumulation time as obtained by Neukum and Hiller (1981). As they demonstrated, the characteristic inflection points at the curve mark the episodes of the most intense destruction of craters, i.e., the resurfacing stages of the Martian surface. When applied to our crater-density curves characterizing the studied areas, this approach allows us to evaluate the absolute model ages for the formation and resurfacing stages of the distinguished stratigraphic units. Our results are presented in the table and illustrated in Figs. 22 and 23.

The estimated age values are highly dispersed for many individual areas (table); moreover, for the studied region as a whole they vary even more, from 4.25 to 0.5 Gyr (Fig. 22). This dispersion apparently reflects the combined effect of two factors: the real existence of several discrete episodes in the resurfacing history
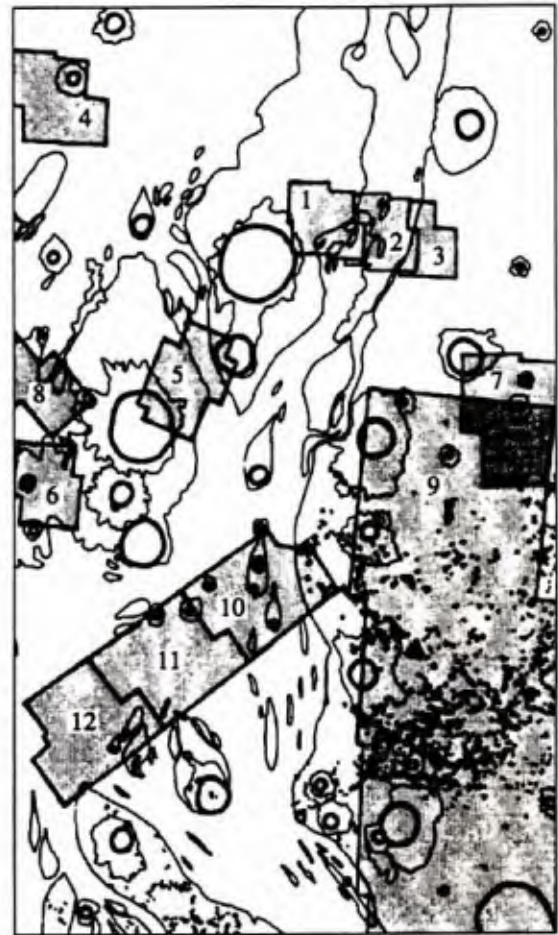
(inflection points at the curves) and stochastic variations related to the high random errors caused by a small volume of data samples.

The wide error intervals for the calculated crater-density values (Fig. 3) result in great uncertainties of age determinations for particular events. We believe, however, that these random errors should be statistically compensated. If this is correct, then individual age values for a given event should form clusters surrounding the true value on the time axis. Actually, in Fig. 22 we can distinguish a group of data points clustering around 3.7 Gyr (it is delimited by a dashed line and includes all valleys and older areas) and another group less distinct and concentrated around 1.5 Gyr. The histogram plotted for the same data (Fig. 23) demonstrates their bimodal or even polymodal structure more clearly. In the histogram, the older, first group of values demonstrates a distinct peak in the range 3.75–4.0 Gyr, whereas in the younger, second group there are three minor peaks marking intervals of 2.25–2.0, 1.75–1.5, and 1.0–0.75 Gyr. In our opinion, these peaks delimit the age ranges for the resurfacing episodes in the region.
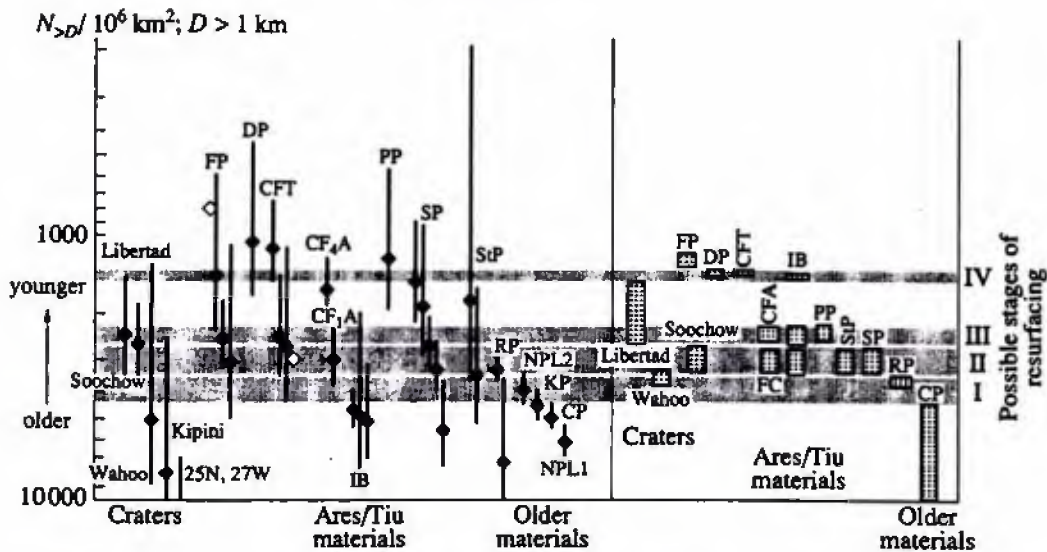
Fig. 21. Stages of resurfacing in the region. Left: ordinates are the cumulative densities of craters greater than 1 km in diameter (solid diamonds); vertical bars show standard deviations; extrapolated values are shown by open diamonds. Right side of the diagram (light gray rectangles) is given according to Fig. 2. Horizontal bands mark the principal stages of resurfacing.

Figure 22 also demonstrates that age estimates for all areas of the oldest stratigraphic units (KP, CP, NPL₁, NPL₂) plot within the oldest interval of the first group (4.25–3.75 Gyr). Values for complex IB₁ fall within only this group. Many other data characterizing either younger areas or those affected by later resurfacing processes (StP, SP, PP, CFA, CFT, FP) plot within both the older and the younger groups, whereas all estimates for dark plains (DP) belong only to the second group. In the case of ridged plains (RP), which seem to be in the intermediate stratigraphic position between ancient and younger areas, three quite similar values are in the center of the first group, and one falls between this and the second group. We interpret this diversity in age determinations as a combination of values characterizing the mapped stratigraphic unit proper, the older underlying materials, and the later resurfacing events— for instance, by persistently active eolian accumulation and erosion, which destroy small craters.

For the oldest surface areas (NPL₁, NPL₂, CP, KP), the crater count turned out to be possible only in low-resolution images. Accordingly, some craters could remain undetected, and age determinations in this case could be younger than the true age of the unit. Another disadvantage of these images is an a fortiori deficiency in the quantity of small craters; consequently, it is impossible to date the resurfacing episodes using the inflection points of the cumulative crater-density curves. In fact, in the second age group, data related to the oldest stratigraphic units are lacking as if these units did not experience later transformations.

The cratered plateau (CP) representing the oldest surface area in the region was apparently formed about 4 Gyr ago; its surface was eroded 3.8–3.7 Gyr ago and

was partially overlapped by the ridged plain (RP) material about 3.7–3.6 Gyr ago. It is difficult to state for certain what peaks in the right part of the histogram (Fig. 23) may mark the particular stages of fluvial activity described above. These stages may be restricted to intervals of 3.6–3.5, 3.5–3.3, 3.0–2.6, 2.3–1.9, and 1.6–1.4 Gyr. The fractured plains (FP) could have been created 1.4–0.6 Gyr ago. The youngest resurfacing stages may be related to episodes of eolian activity and local thermokarst reworking.

The ages of the Ares and Tiu Valles were estimated to correspond to 3.65–2.5 and 3.5–2.0 Gyr (Neukum and Hiller, 1981). Using the same approach to the interpretation of the crater-density distribution, Robinson *et al.*, (1996) concluded that some areas of the Ares Vallis were mainly formed prior to 3.5 Gyr, and their later reworking took place between 2.21 and 1.66 Gyr. Our age estimates characterizing the formation period and subsequent resurfacing stages of the Ares and Tiu Valles are thus concordant in general with the quoted data.

In summary, let us compare the dating results with the outlined stratigraphic relations. According to the stratigraphic data, the studied region went through several stages of resurfacing. The estimated absolute ages of individual stratigraphic units suggest this scenario, virtually, for each of them.

7. A RECONSTRUCTION OF THE GEOLOGICAL HISTORY OF THE REGION

The results of this study and the data published before allow us to argue for the following scenario of geological history in the Ares and Tiu Valles region.
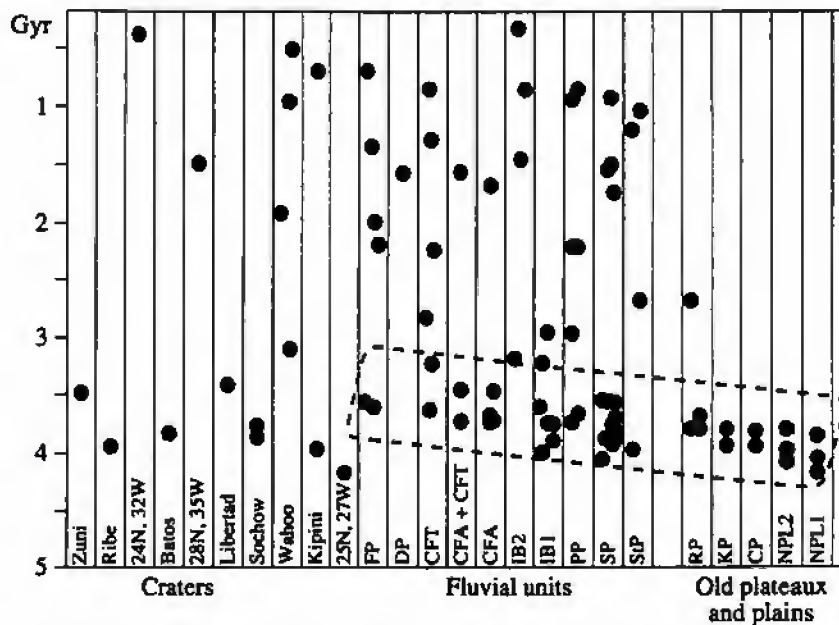
Fig. 22. Estimated absolute-age values (solid circles) for the distinguished stratigraphic units, arranged along the horizontal axis in the same succession as in Figs. 2 and 21. Inside the vertical columns, dots corresponding to the same area are placed strongly above one another; dots are slightly displaced in the horizontal direction with respect to one another to denote different areas of the same unit.

The lithologic unit of the cratered plateau (CP) was formed here, as in many other regions of Mars, during the Noachian time (about 4 Gyr ago; see Fig 24a). This plateau is thought to be composed of impact breccias and ancient lavas (Rotto and Tanaka, 1995). The Ares and Tiu Valles open into the impact depression of the Chryse Planitia impact basin that was also formed at the Noachian time (Schultz *et al.*, 1982). A considerable subsidence in the northern hemisphere of Mars and the formation of northern lowlands is attributed to the end of the Noachian period (McGill and Dimitriou, 1990). In the studied region, these events created an escarpment at the northern boundary of the cratered plateau, and this structural feature subsequently retreated southward under the influence of slope-collapse events and water-saturated mudflows. As a result, the ancient cratered plateau was under destruction in the north, leaving behind the knob-plateau unit (KP), hills (H), and remnants of ancient craters in the form of rings of knobs (RK). This was resurfacing stage I of the region. It is likely that, during this time (3.8–3.7 Gyr ago), there were also fluvial valleys or their systems in the region, but their traces are destroyed. Close to this period (3.7–3.6 Gyr ago), the surface between the hills was covered with the material of ridged plains (RP, Fig. 24b), i.e., with lavas and/or sedimentary materials transported from the eroded plateaux.

Afterward, but still at the end of the Noachian time and during the first half of the Hesperian period, a giant catastrophic outflow arose from an underground reservoir located far to the south. Originally, its flows meandered over the plains, eroded them along a wide front,

and deposited their material in faint valleys (FC); later, they were concentrated in the present-day valleys to form their upper benches. The outflow deltaic sediments represent the material of spotted (StP) and smooth (SP) plains (Fig. 24c). The sedimentary cover, almost uniform in thickness (dozens of meters), overlies the impact craters, thus implying that deltaic materials were probably accumulated over a vast area of a temporary sea. This was resurfacing stage II of the region.

After a time interval of unknown duration, there was another cycle of catastrophic floods in the Hesperian
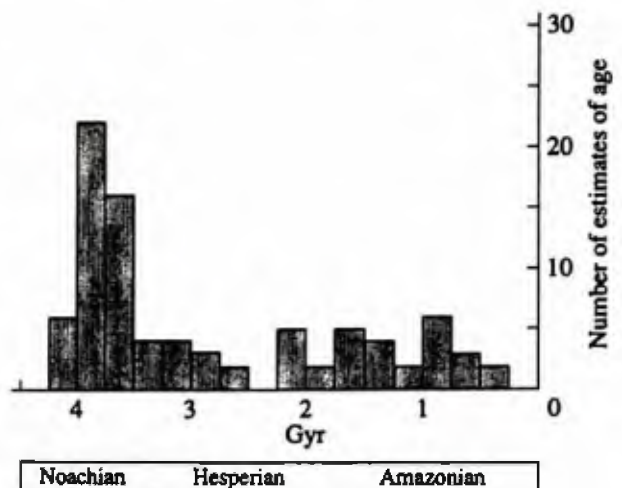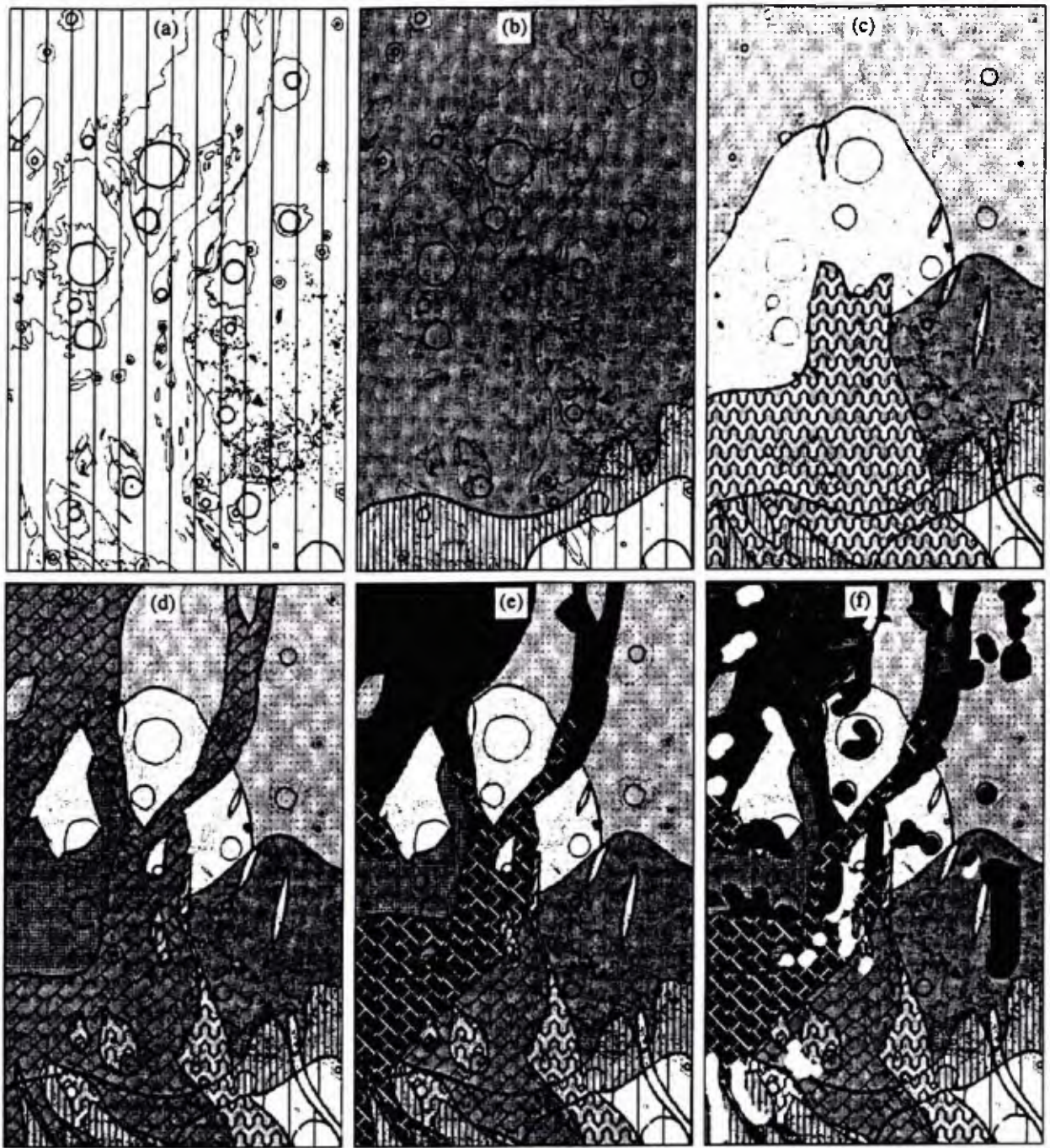

Fig. 23. Histogram of age estimates (the same as in Fig. 22); main epochs of Martian stratigraphy from Hartmann (1981).
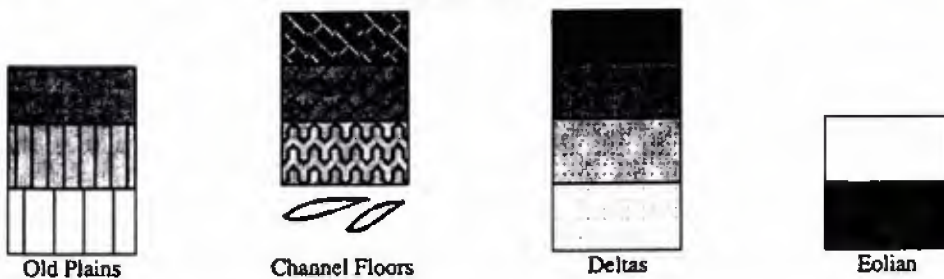
MATERIALS:

Old Plains   Channel Floors   Deltas   Eolian

Fig. 24. Schemes illustrating the reconstruction of the geological history of the studied region. Present-day position of large impact craters and valley boundaries is shown in all figures.

period—resurfacing stage III. This event deepened the valleys, and deltaic deposits of the preceding stage were eroded by newly born flows. We consider this stage as the formation period of pitted plains (PP) with frequent rounded cauldrons. Some researchers believe that these cauldrons are similar to terrestrial thermokarst landforms—alases (Costard and Kargel, 1995). This stage was terminal for the fluvial reworking of the Ares floor material (CFA, Fig. 24d) and might be initial for the Tiu Vallis formation. Moreover, the Tiu Vallis floor is incised into the floor of the Ares Vallis, and the crater density in the former is less than in the latter. This suggests that the Tiu Vallis was affected by a later episode of fluvial activity separated from the described one by a considerable time gap.

During the next Late Hesperian–Early Amazonian period (resurfacing stage IV), the incision of the Tiu Vallis was further in progress, the material of pitted plains was heavily eroded, and remnants of the latter are represented now by benches and islands. Likely, the Tiu Vallis of that time was the only route for run-off, and fluvial processes completed the formation of the valley-floor deposits.

Plains with furrows, wrinkle ridges, and fractures (FP) may also be related in origin to the last stage of fluvial activity, as these landforms probably appeared as a result of exsiccation, freezing, and consolidation of sediments (Jöns, 1986; McGill and Hills, 1992; Parker et al., 1993; Tanaka, 1997). In the opinion of Tanaka (1995, 1997), the material of these plains was disturbed by return flows and invaded the terminal areas of the valleys (Fig. 24e). It is also possible that the FP material was brought from another outflow valley, located outside the region.

Eolian and slope processes along with impact cratering developed throughout the entire geological history of the region (Fig. 24f); they are active even at present.

9. CONCLUSION

Our purpose in this work was to answer the questions of how, from where, and when various materials appeared in the exploration region of the Mars Pathfinder rover (Fig. 1a). This region is at the boundary between the lithologic units of the Ares (CFA) and Tiu (CFT) Valles (the latter being younger than the former) that we have mapped. According to the morphology, this part of the Tiu Vallis floor is classed with smooth floor plains (type CF_1).

We believe that both valleys and their lithologic units were related in origin to the fluvial activity of several catastrophic floods.

Deposits in the mouth of the valleys should consist of two groups of materials transported by the flows. First, they should incorporate a more ancient material derived from the cratered and knobby plateaux, from hills, and from other units (not studied by us) located to the south of the region. This is the material of ancient highland terrains (presumably, impact breccias and lavas). Second, a younger sedimentary, volcanic, or volcano-sedimentary material of ridged plains should be present. The material transported by water-saturated flows must be influenced by mechanical reworking, i.e., the fragments must be rounded, sorted, etc. Judging from the first published results obtained by the Mars Pathfinder rover, these features are actually visible (Golombek et al., 1997a; Matijevic et al., 1997). The material of ejecta from impact craters, nearby and distant, should also be present at the surface; however, it should not bear signs of fluvial reworking. In addition, the material at the rover-operation site must include dark eolian sand and bright dust.

When were the deposits studied by the rover formed? According to our appraisal, the lithologic units of plateaux were formed about 4 Gyr ago and those of ridged plains approximately 3.5 Gyr ago. Thus, they are very ancient, and the fluvial reworking of these units took place first between 3.6 and 2.6 Gyr ago and then, presumably, between 2.3 and 1.4 Gyr ago. When the fluvial activity ceased, the floor deposits experienced wind erosion, which was apparently not very intense (Golombek et al., 1997a; Matijevic et al., 1997; Smith et al., 1997; Basilevsky et al., 1998), and, possibly, thermokarst resurfacing. Finally, all these formations were locally overlain by eolian dust and sand, and also by ejecta from impact craters.

ACKNOWLEDGMENTS

REFERENCES

Arvidson, R., Wind-Blown Streaks, Splotches and Associated Craters on Mars: Statistical Analysis of Mariner 9 Photographs, Icarus, 1974, vol. 21, pp. 12–27.

Arvidson, R., Guinness, E.A., and Zent, A.P., Classification of Surface Units in the Equatorial Region of Mars Based on Viking Orbiter Color, Albedo, and Thermal Data, J. Geophys. Res., 1982, vol. 87, pp. 10149–10157.

Arvidson, R., Guinness, E.A., Dale-Bannister, M.A., Adams, J., Smith, M., Christensen, P.R., and Singer, R., Nature and Distribution of Surficial Deposits in Chryse Planitia and Vicinity, Mars, J. Geophys. Res., 1989, vol. 94, pp. 1573–1587.

Baker, V.R. and Milton, D.J., Erosion by Catastrophic Floods on Mars and on Earth, Icarus, 1974, vol. 23, pp. 27–41.

Baker, V.R. and Kochel, R.C., Morphological Mapping of Martian Outflow Channels, Proc. Lunar Sci. Conf. IX, 1978, pp. 3181–3192.

Baker, V.R. and Kochel, R.C., Martian Channel Morphology: Maja and Kasei Valles, J. Geophys. Res., 1979, vol. 84, pp. 7961–7983.

Baker, V.R., The Channels of Mars, Austin: Univ. of Texas Press, 1982.

Baker, V.R., Strom, R.G., Gulick, V.C., Kargel, J.S., Komatsu, G., and Kale, V.S., Ancient Oceans, Ice Sheets and the Hydrological Cycle of Mars, *Nature*, 1991, vol. 352, pp. 589–594.

Basilevsky, A.T., Markiewicz, W.J., and Keller, H.U., Morphology of Rocks within and nearby Rock Garden: *Mars Pathfinder* Landing Site, *Abstr. Lunar Planet. Sci. Conf. XXIX*, 1998, no. 1378 (CD-ROM).

Betts, B.H. and Murray, B.C., Thermal Studies of Martian Channels and Valleys Using Termoskan Data, *Abstr. Lunar Planet. Sci. Conf. XXIV*, 1993, pp. 103–104.

Bretz, J.H., Smith, H.T.U., and Neff, G.E., Channeled Scabland of Washington: New Data and Interpretations, *Bull. Geol. Soc. Am.*, 1956, vol. 67, pp. 957–1049.

Bretz, J.H., The Lake Missoula Floods and the Channeled Scabland, *J. Geol.*, 1969, vol. 77, pp. 505–543.

Butvilovskii, V.V., *Paleogeografiya poslednego oledeneniya i Golotsena Altaya: Sobytiino-katastroficheskaya model'* (Last Glaciation and Holocene Paleogeography of Altai: Catastrophic-Event Model), Tomsk: Tomsk. Univ., 1993.

Carr, M.H., Crumpler, L.S., Cutts, J.A., Greeley, R., Guest, J.E., and Masursky, H., Martian Impact Craters and Emplacement of Ejecta by Surface Flow, *J. Geophys. Res.*, 1977, vol. 82, pp. 4055–4065.

Carr, M.H., Formation of Martian Flood Features by Release of Water from Confined Aquifers, *J. Geophys. Res.*, 1979, vol. 84, pp. 2995–3007.

Carr, M.H., *Water on Mars*, New York: Oxford Univ. Press, 1996.

Christensen, P.R., Martian Dust Mantling and Surface Composition: Interpretation of Thermophysical Properties, *J. Geophys. Res.*, 1982, vol. 87, pp. 9985–9998.

Christensen, P.R., The Spatial Distribution of Rocks on Mars, *Icarus*, 1986, vol. 68, pp. 217–238.

Christensen, P.R. and Kieffer, H.H., Moderate Resolution Thermal Mapping of Mars: the Channel Terrain around Chryse Basin, *J. Geophys. Res.*, 1989, vol. 94, pp. 8233–8238.

Costard, F., Unusual Concentration of Rampart Craters at the Mouths of Outflow Channels, Mars, *Abstr. Lunar Planet. Sci. Conf. XXV*, 1994, pp. 287–288.

Costard, F. and Baker, V., Thermokarst Landforms and Processes in Ares Vallis, Mars, *Abstr. Lunar Planet. Sci. Conf. XXVI*, 1995, pp. 285–286.

Costard, F.M. and Kargel, J.S., Outwash Plains and Thermokarst on Mars, *Icarus*, 1995, vol. 114, pp. 93–112.

Craddock, R.A., Crumpler, L.S., Aubele, J.C., and Zimbelman, J.R., Geology of Central Chryse Planitia and the *Viking 1* Landing Site: Implications for the *Mars Pathfinder* Mission, *J. Geophys. Res.*, 1997, vol. 102, no. E2, pp. 4161–4183.

Crumpler, L.S., Geologic Mapping Traverse of the Highland-to-Lowland Transition in an Area Adjacent to the *Mars Pathfinder* Region, *Lunar Planet. Inst. Tech. Rep.*, 1995, vol. 95-1, pp. 10–11.

De Hon, R.A., Flood Surge in Martian Outflow System: Episodic Flow, *Abstr. Lunar Planet. Sci. Conf. XX*, 1989, pp. 230–231.

Edgett, K.S. and Christensen, P.R., The Particle Size of Martian Aeolian Dunes, *J. Geophys. Res.*, 1991, vol. 96, pp. 22765–22776.

Edgett, K.S. and Christensen, P.R., Mars Aeolian Sand: Regional Variations Among Dark-Hued Crater Floor Features, *J. Geophys. Res.*, 1994, vol. 99, pp. 1997–2018.

Edgett, K.S. and Christensen, P.R., Rocks and Aeolian Features in the *Mars Pathfinder* Landing Site Region: *Viking* Infrared Thermal Mapper Observations, *J. Geophys. Res.*, 1997, vol. 102, pp. 4107–4116.

Golombek, M.P., Parker, T.J., and Moore, H.J., *Mars Pathfinder* Landing Site Characteristics, *Abstr. Lunar Planet. Sci. Conf. XXVI*, 1995, pp. 481–482.

Golombek, M.P., Cook, R.A., Economou, T., Folkner, W.M., Haldemann, A.F.C., Kallemeyn, P.H., Knudsen, J.M., Manning, R.M., Moore, H.J., Parker, T.J., Rieder, R., Schofield, J.T., Smith, P.H., and Vaughan, R.M., Overview of the *Mars Pathfinder* Mission and Assessment of Landing Site Predictions, *Science*, 1997a, vol. 278, pp. 1743–1748.

Golombek, M.P., Cook, R.A., Moore, H.J., and Parker, T.J., Selection of the *Mars Pathfinder* Landing Site, *J. Geophys. Res.*, 1997b, vol. 102, no. E2, pp. 3967–3988.

Hamblin, W.K., *The Earth's Dynamic Systems*, Minneapolis: Burgess, 1975.

Hartmann, W.K., Strom, R.G., Weidenschilling, S.J., Balsius, K.R., Woronow, A., Dence, M.R., Grieve, R.A.F., Diaz, J., Chapman, C.R., Shoemaker, E.M., and Jones K.L., Chronology of Planetary Volcanism by Comparative Studies of Planetary Cratering, in *Basaltic Volcanism on the Terrestrial Planets*, New York: Pergamon, 1981, pp. 1049–1128.

Jöns, H.-P., Sedimentary Basins and Mud Flows in the Northern Lowlands of Mars, *Abstr. Lunar Planet. Sci. Conf. XV*, 1984, pp. 417–418.

Jöns, H.-P., Late Sedimentation and Late Sediments in the Northern Lowlands on Mars, *Abstr. Lunar Planet. Sci. Conf. XVI*, 1985, pp. 414–415.

Jöns, H.-P., Arcuate Ground Undulations. Gelifluxion-like Features and "Front Tori" in the Northern Lowlands on Mars—What do They Indicate? *Abstr. Lunar Planet. Sci. Conf. XVII*, 1986, pp. 404–405.

Kargel, J.S., Baker, V.R., Begét, J.E., Lockwood, J.F., Pewé, T.I., Shaw, J., and Strom, R.G., Evidence of Ancient Continental Glaciation in the Martian Northern Plains, *J. Geophys. Res.*, 1995, vol. 100, no. E3, pp. 5351–5369.

Komatsu, G., Baker, V.R., and Johnson, J.R., Ares Vallis: Flood Geomorphology of *Mars Pathfinder* Landing Site, *Abstr. Lunar Planet. Sci. Conf. XXVI*, 1995, pp. 779–780.

Komatsu, G. and Baker, V.R., Paleohydrology and Flood Geomorphology of Ares Vallis, *J. Geophys. Res.*, 1997, vol. 102, no. E2, pp. 4151–4160.

Kuz'min, R.O., Determination of the Occurrence Depth of Ice-Bearing Rocks on Mars from Morphology of Young Craters, *Dokl. Akad. Nauk SSSR*, 1980, vol. 252, no. 6, pp. 1445–1448.

Kuzmin, R.O. and Greeley, R., Geology of *Mars-Pathfinder* Landing Site Ellipse, in *Abstracts of Papers Submitted to*

the 22 Russian–American Microsymposium on Comparative Planetology, Moscow, 1995a, pp. 51–52.

Kuzmin, R.O. and Greeley, R., Geology of the Landing Site Ellipse, *Lunar Planet. Inst. Tech. Rep.*, 1995b, vol. 95-01, pp. 20–21.

Kuz'min, R.O., private communication, 1996.

Lucchitta, B.K., Anderson, D.M., and Shoji, H., Did Ice Streams Carve Martian Outflow Channels?, *Nature*, 1981, vol. 290, no. 5809, pp. 759–763.

Lucchitta, B.K., Ice Sculpture in the Martian Outflow Channels, *J. Geophys. Res.*, 1982, vol. 87, pp. 9951–9973.

Lucchitta, B.K., Ice and Debris in the Fretted Terrain, Mars, *Proc. Lunar Planet. Sci. Conf. XIV*, 1984, pp. B409–B418.

Lucchitta, B.K., Ferguson, H.M., and Summers, C., Sedimentary Deposits in the Northern Lowland Plains, Mars, *J. Geophys. Res.*, 1986, vol. 91E, pp. 166–174.

Marchenko, A.G., Geologic Mapping of the Mouth of Ares Vallis, Mars: Preliminary Results, in *Abstracts of Papers Submitted to the 24th International Microsymposium on Planetology*, Moscow, 1996, pp. 62–63.

Marchenko, A.G., Basilevsky, A.T., Neukum, G., and Hoffmann, H., Crater Counting in Three Areas of Ares Vallis, *Space Planet. Sci. (Ann. Geophys.)*, 1996, vol. 14, Suppl. III, p. C792.

Marchenko, A.G., Basilevsky, A.T., Neukum, G., Hauber, E., Hoffmann, H., and Cook, A.C., Mapping of the Mouth of Ares Vallis, Mars, *Abstr. Lunar Planet. Sci. Conf. XXVIII*, 1997, pp. 865–866.

Marchenko, A.G., Basilevsky, A.T., Neukum, G., Hauber, E., Hoffmann, H., and Cook, A.C., The Study of the Mouth of Ares and Tiu Valles, Mars, *Abstr. Lunar Planet. Sci. Conf. XXIX*, 1998, no. 1174 (CD-ROM).

Masursky, H., Boys, J.M., Dial, A.L., Shauber, G.G., and Strobel, M.E., Classification and Time of Formation of Martian Channels Based on *Viking* Data, *J. Geophys. Res.*, 1977, vol. 82, pp. 4016–4038.

Matijevic, J.R., Crisp, J., *et al.*, Characterization of the Martian Surface Deposits by the *Mars Pathfinder* Rover, Sojourner, *Science*, 1997, vol. 278, pp. 1765–1768.

McCauley, J.F., Carr, M.H., Cutts, J.A., Hartmann, W.K., Masursky, H., Milton, D.J., Sharp, R.P., and Wilhelms, D.E., Preliminary *Mariner 9* Report on the Geology of Mars, *Icarus*, 1972, vol. 17, pp. 289–327.

McGill, G.E. and Dimitriou, A.M., Origin of the Martian Global Dichotomy by Crustal Thinning in the Late Noachian or Early Hesperian, *J. Geophys. Res.*, 1990, vol. 95, pp. 12595–12605.

McGill, G.E. and Hills, L.S., Origin of Giant Martian Polygons, *J. Geophys. Res.*, 1992, vol. 97, pp. 2633–2647.

Milton, D.J., Water and Processes of Degradation in the Martian Landscape, *J. Geophys. Res.*, 1973, vol. 78, pp. 4037–4047.

Mustard, J.F., Are Dark Red Soils and Bright Dust on Mars Related through Mineralogic Phase Changes? *Abstr. Lunar Planet. Sci. Conf. XXVI*, 1995, pp. 1021–1022.

Nelson, D.M. and Greeley, R., Geologic Sequence of Formation and Evidence for Sheetwash Erosion at the Ares Vallis Region, Mars, *Abstr. Lunar Planet. Sci.*, 1996, pp. 945–946.

Nelson, D.M. and Greeley, R., Xante Terra Outflow Channel Geology at the Mars Pathfinder Landing Site, *Abstr. Lunar Planet. Sci. Conf. XXIX*, 1998, no. 1158 (CD-ROM).

Neukum, G. and Wise, D.U., Mars: a Standard Crater Curve and Possible New Time Scale, *Science*, 1976, vol. 194, pp. 1381–1387.

Neukum, G. and Hiller, K., Martian Ages, *J. Geophys. Res.*, 1981, vol. 86, pp. 3097–3121.

Nummedal, D. and Prior, D.B., Generation of Martian Chaos and Channels by Debris Flows, *Icarus*, 1981, vol. 45, pp. 77–86.

Parker, T.J., Saunders, R.S., and Schneeberger, D.M., Transitional Morphology in the West Deuteronilus Mensae Region of Mars: Implications for Modification of the Uplands/Lowlands Boundary, *Icarus*, 1989, vol. 82, pp. 111–145.

Parker, T.J., Gorsline, D.S., Saunders, R.S., Pieri, D.C., and Schneeberger, D.M., Coastal Geomorphology of the Martian Northern Plains, *J. Geophys. Res.*, 1993, vol. 98, pp. 11061–110878.

Pike, R.J. and Davis, P.A., Toward a Topographic Model of Martian Craters from Photoclinometry, *Abstr. Lunar Planet. Sci. Conf. XV*, 1984, pp. 645–646.

Rice, J.W., Jr. and De Hon, R.A., *Geologic Map of the Darvel Quadrangle, Maja Vallis Region, Mars*, USGS Map I-2432, 1 : 500000, 1996.

Rice, J.W., Jr. and Edgett, K.S., Catastrophic Flood Sediment in Chryse Basin, Mars, and Quincy Basin, Washington: Application of Sandar Facies Model, *J. Geophys. Res.*, 1997, vol. 102, pp. 4185–4200.

Robinson, C.A., Neukum, G., Hoffmann, H., Marchenko, A., Basilevsky, A.T., and Ori, G.G., Suggested Geological Development for Ares Vallis, Mars, *Abstr. Lunar Planet. Sci. Conf. XXVII*, 1996, pp. 1083–1084.

Rotto, S. and Tanaka, K.L., *Geologic/Geomorphologic Map of the Chryse Planitia region of Mars*, USGS Map I-2441, 1 : 5000000, 1995.

Rudoi, A.N., Geomorphological Effect and Hydraulics of the Late Pleistocene Jökulhlaups of Ice-Dammed Lakes, Altai, *Geomorfologiya*, 1995, no. 4, pp. 61–76.

Schultz, P.H., Schultz, R.A., and Rogers, J., The Structure and Evolution of Ancient Impact Basins on Mars, *J. Geophys. Res.*, 1982, vol. 87, pp. 9803–9820.

Scott, D.H. and Carr, M.H., *Geologic Map of Mars*, USGS Map I-1083, 1 : 25000000, 1978.

Scott, D.H., Schaber, G.G., Horstman, K.C., and Dial, A.L., Jr., Lava Flows of Tharsis Montes, *NASA Tech. Memo*, 1979, vol. 80339, pp. 237–238.

Scott, D.H., Meander Relics: Evidence of Extensive Flooding on Mars, *NASA Tech. Memo*, 1982, vol. 85127, pp. 216–218.

Scott, D.H. and Tanaka, K.L., *Geologic Map of the Western Equatorial Region of Mars*, USGS Map I-1802-A., 1 : 15000000, 1986.

Scott, D.H., Rice, J.W., Jr., and Dohm, J.M., Paleolakes and Lacustrine Basins on Mars, *Abstr. Lunar Planet. Sci. Conf. XXII*, 1991, pp. 1203–1204.

Scott, D.H., Dohm, J.M., and Rice, J.W., Jr., *Map of Mars Showing Channels and Possible Paleolake Basins*, USGS Map I-2461, 1 : 30000000, 1995.

Sharp, R.P. and Malin, M.C., Channels on Mars, *Bull. Geol. Soc. Am.*, 1975, vol. 86, pp. 593–609.

Smith, P.H., Bell, J.F. III., Bridges, N.T., *et al.*, Results from the *Mars Pathfinder* Camera, *Science*, 1997, vol. 278, pp. 1758–1764.

Soderblom, L.A., Edwards, K., Eliason, E.M., Sachez, E.M., and Charette, M.P., Color Variations on the Martian Surface, *Icarus*, 1978, vol. 34, pp. 446–464.

Squyres, S.W. and Kasting, J.F., Early Mars: How Warm and How Wet?, *Science*, 1994, vol. 265, pp. 744–749.

Tanaka, K.L., Chaotic Material and Debris Flows in the Simud-Tiu Valley Outflow System of Mars, *Abstr. Lunar Planet. Sci. Conf. XIX*, 1988, pp. 1175–1176.

Tanaka, K.L., Geologic History of Chryse Basin, Mars, *Lunar Planet. Inst. Tech. Rep.*, 1995, vol. 95-01, pp. 39–40.

Tanaka, K.L., Sedimentary History and Mass Flow Structures of Chryse and Acidalia Planitiae, Mars, *J. Geophys. Res.*, 1997, vol. 102, no. E2, pp. 4131–4149.

Thórarinsson, S., The Jökulhlaup From the Katla Area in 1955 Compared with Other Jökulhlaups in Iceland, *Jökull*, 1957, vol. 7, pp. 21–25.

Thornhill, G.D., Rothery, D.A., Murray, J.B., Cook, A.C., Day, T., Muller, J.P., and Iliffe, J.C., Topography of Apollinaris Patera and Ma'adim Vallis: Automated Extraction of Digital Elevation Models, *J. Geophys. Res.*, 1993, vol. 98, no. E12, pp. 23581–23587.

Treiman, A.H., Hardpan and Other Diagenetic "Rock" in the Catchment of Ares Vallis and Surrounding Areas, *Lunar Planet. Inst. Tech. Rep.*, 1995, no. 95-01, pp. 28–29.

Treiman, A.H., What Is Mars' Highlands Crust?, in *Conference on Early Mars: Geologic and Hydrologic Evolution, Physical and Chemical Environments, and Implications for Life*, Houston, 1997, pp. 77–78.

Watters, T.R., Wrinkle Ridge Assemblages on the Terrestrial Planets, *J. Geophys. Res.*, 1988, vol. 93, pp. 10236–10254.

Wise, D.U., Golombek, M. P., and McGill, G.E., Tharsis Province of Mars: Geologic Sequence, Geometry, and a Deformation Mechanism, *Icarus*, 1979, vol. 38, pp. 456–472.